Journal of Modern Physics, 2025, 16(8), 1084-1123
https://www.scirp.org/journal/jmp
ISSN Online: 2153-120X
ISSN Print: 2153-1196

Geometric Deformation Wave Model of Brane Cosmology: A Unified Origin of Gravitation, Matter, Dark Matter and Dark Energy

Owen Xie[1], Fengchun Xie[2]

[1]East Chapel Hill High School, Chapel Hill, NC, USA
[2]School of Chemistry and Chemical Engineering, South China University of Technology, Guangzhou, China
Email: owenxie550@gmail.com, acfchxie@scut.edu.cn

How to cite this paper: Xie, O. and Xie, F.C. (2025) Geometric Deformation Wave Model of Brane Cosmology: A Unified Origin of Gravitation, Matter, Dark Matter and Dark Energy. *Journal of Modern Physics*, **16**, 1084-1123.
https://doi.org/10.4236/jmp.2025.168056

Received: July 14, 2025
Accepted: August 5, 2025
Published: August 8, 2025

Abstract

We introduce a deformation wave model of brane cosmology, where a 5D membrane embedded in a 6D bulk spacetime undergoes intrinsic geometric deformations triggered by a Gaussian perturbation. This process drives a three-stage cosmic evolution—inflation zone, transition, and membrane oscillation—forming a "universe factory" that generates stable 4D universes at wave crests (matter-dominated) and troughs (antimatter-dominated). The Einstein Field Equations (EFE) are derived geometrically from the brane's elastic dynamics, without invoking traditional inflation-like scalar fields, providing a physical mechanism for spacetime curvature. Dark energy emerges from the membrane's intrinsic wave speed, yielding a constant density incorporated $\Lambda h_{\mu\nu}$ as in the EFE, consistent with late-time acceleration ($\Omega_\Lambda = 0.7$). Dark matter arises as the predecessor universes gravity traces in dark sectors, reproducing galactic ratios ($\frac{\rho_{DM}}{\rho_b} \approx 5$). The model aligns with CMB observations ($n_s = 0.96$) and predicts a finite multiverse with testable CMB anisotropies. This framework unifies gravity, dark matter, and dark energy geometrically, offering a physically grounded alternative to standard brane inflation and ΛCDM.

Keywords

Brane Cosmology, Deformation Wave, Geometric Gravity, Dark Energy, Dark Matter

1. Introduction

Higher-dimensional theories, deeply rooted in string theory and M-theory [1]-

[3], have significantly reshaped modern cosmology by proposing that our observable 4D universe exists as a brane—a lower-dimensional hypersurface—embedded within a higher-dimensional bulk spacetime [4] [5]. These brane-world scenarios have provided fertile ground for addressing longstanding puzzles in physics, such as the hierarchy problem, which questions the vast disparity between the electroweak scale and the Planck scale, and the cosmological constant problem, which seeks to explain the tiny yet non-zero value of dark energy driving cosmic acceleration [6]. Observational evidence, including precise measurements of the cosmic microwave background (CMB) power spectrum with a scalar spectral index $n_s \approx 0.96$ [7], has lent credence to inflationary models within such frameworks, suggesting that the early universe underwent rapid expansion seeded by quantum fluctuations. However, conventional brane-world models often rely on additional scalar fields (e.g., inflations) or inter-brane interactions to drive inflation and cosmic evolution, leaving critical questions unresolved: What is the physical origin of gravity as described by General Relativity (GR)? How do dark matter and dark energy emerge naturally within a unified framework?

In this work, we propose a novel deformation wave model of brane cosmology to address these fundamental issues, and focus primarily on deriving the gravitational field equations from the deformation wave model. While we provide a qualitative discussion on the origins of dark energy and dark matter within this framework, a full quantitative analysis requires further refinement of the dynamical equations, which we leave for future studies. The goal of this paper is to establish a theoretical foundation, ensuring that the proposed model is mathematically consistent and aligns qualitatively with observational data. Our approach posits that a 5D membrane, embedded in a 6D bulk spacetime, undergoes dynamic geometric deformations initiated by a Gaussian perturbation along the extra dimensions. Unlike traditional models that introduce inflation-like scalar fields or fine-tuned potentials, our framework derives the EFE directly from the brane's deformation wave, characterized by the geometric field $\Phi = A\left(x^{\mu}\right)\cos\left(k_{wave}x^4 - \omega t + \varphi\right)$, $\left(\mu = 0,1,2,3,4\right)$ or brane's intrinsic elastic properties, offering a purely geometric origin for gravity. In our model, all matter and energy in the universe comes from the brane deformation, and the curvature of space-time in the universe originates from the brane deformation. Undamped propagation of brane deformation waves ensures the conservation of mass and energy in the universe. Traditional brane models, such as the Dvali-Gabadadze-Porrati (DGP) [8] and Randall-Sundrum (RS) [9] frameworks, often rely on additional scalar fields or fine-tuned assumptions about the bulk geometry to stabilize the brane and reproduce gravitational effects.

The geometric deformation wave propagates across the brane, driving a three-stage cosmic evolution: an initial inflation zone dominated by rapid expansion, a transition phase that generates observable universes where the wave stabilizes, and a membrane oscillation phase. At the wave's crests and troughs—regions where the kinetic energy of the deformation vanishes—stable 4D spacetimes emerge, with crests hosting matter-dominated universes and troughs potentially forming antimatter-dominated counterparts. This cyclic process acts as a "universe factory," producing a finite multiverse with distinct physical properties testable through CMB anisotropies.

The model's geometric foundation extends beyond gravity to encompass the origins of dark matter and dark energy. In the interstitial dark sectors between crests and troughs, where the deformation gradient $\partial_4 \Phi \neq 0$ is significant, gauge field instabilities trigger energy storms—localized bursts of energy that dissipate over time. These energy storms disrupt small-scale spacetime curvature traces (e.g., stellar scales) in dark sectors, preventing observable dark matter effects at these scales, while galaxy-scale traces persist as the source of dark matter gravity since the energy storms can't continuously amplify very long, which accumulate across oscillation cycles to form dark matter, contributing an energy density ratio consistent with galactic observations ($\frac{\rho_{DM}}{\rho_b} \approx 5$) [10]. Simultaneously, dark energy arises from the membrane's intrinsic wave speed, defined as $C_{membrane} = \sqrt{\frac{T}{\rho}}$, where T is the brane's bulk modulus and ρ is its surface density. This wave speed induces a constant energy density $\rho_{DE} = \frac{3T}{8\pi G R_0^2 \rho}$, incorporated into the EFE as a cosmological constant-like term $\Lambda h_{\mu\nu}$, driving latetime cosmic acceleration in agreement with the observed dark energy fraction ($\Omega_\Lambda \approx 0.7$) [11]. By deriving these components geometrically, our model eliminates the need for ad hoc fields or parameters.

This approach not only aligns with cornerstone cosmological observations—such as the CMB spectral index $n_s \approx 0.96$ from Planck data [7] and the dark matter-to-baryon ratio from large-scale structure surveys [10]—but also offers a predictive framework for future experiments. The distribution of dark matter encodes signatures of the pre-multiverse, potentially observable with next-generation telescopes. Furthermore, by unifying gravity, dark matter, and dark energy within a single geometric construct, our model contrasts with standard paradigms like CDM and brane inflation, which rely on separate postulates for each phenomenon [6] [12].

To elucidate these ideas, the paper is structured as follows: Section 2 establishes the mathematical framework, including the brane's geometry and deformation dynamics; Section 3 details the three-stage cosmic evolution (3.1), gauge field stability and energy storms (3.2), the EFE derivation from and dark sector contributions (3.3); Section 4 concludes with insights, comparisons to existing models, and directions for future research.

This paper proposes a preliminary deformation wave model aimed at providing a unified geometric interpretation for the origins of gravity, dark matter, and dark energy, with future quantitative analyses to further validate its predictions.

2. Mathematical Foundations

In this section, we establish the core mathematical structure underlying our brane-cosmology framework and the associated deformation-wave model. We first specify the dimensional setup and the relevant fields, then formulate the membrane (brane) action and the bulk action, and finally incorporate the initial Gaussian perturbation that triggers the membrane deformation field (or wave) leading to inflationary dynamics and subsequent ripple propagation.

2.1. Effective Metric and Spacetime Structure

To properly describe the physics of a 5D membrane embedded in a 6D higher-dimensional bulk space, the induced metric on the membrane must be defined first. The 6D background bulk spacetime metric in higher dimensions is given by [13]:

$$g_{MN}^{(6)} \mathrm{d}x^M \mathrm{d}x^N = g_{ab}^{(5)} \mathrm{d}x^a \mathrm{d}x^b + \mathrm{d}y^2 \tag{1}$$

where the induced 5D brane metric is derived from the bulk metric via [14]:

$$g_{ab}^{(5)} = g_{MN}^{(6)} \frac{\partial x^M}{\partial \xi^a} \frac{\partial x^N}{\partial \xi^b} \tag{2}$$

The 4D metric of the observable universe is extracted as [13]:

$$h_{\mu\nu} = g_{ab}^{(5)} \frac{\partial \xi^a}{\partial x^\mu} \frac{\partial \xi^b}{\partial x^\nu}. \tag{3}$$

These reductions establish the basis for translating higher-dimensional geometric effects into 4D observable phenomena [15].

2.2. Deformation Waves and Brane Geometry

The deformation waves are undamped longitudinal waves; the deformation wave field equation is given by:

$$\Phi = A\left(x^\mu\right)\cos\left(k_{wave} x^4 - \omega t + \varphi\right), \left(\mu = 0,1,2,3,4\right) \tag{4}$$

where:

- Φ is the measure of deformation, and the only direction of Φ is the direction of propagation of the deformation wave.
- x^μ is the brane spacetime coordinate.
- x^4 is the space coordinate of the propagation direction.
- t is the time coordinate.
- k_{wave} is the wave number.
- ω is the wave angular frequency.
- φ is the wave initial phase.
- $A\left(x^\mu\right)$ is the wave amplitude.

The deformation field Φ in our model is not only a classical wave but also exhibits microscopic quantum characteristics through its localized structures, termed deformation "knots." These knots are quantized excitations of the field Φ

at its extrema—namely the crests and troughs of the deformation wave—it forms localized structures known as deformation knots. These knots represent the geometric origin of matter particles, with their energy concentrated in specific regions rather than dispersing across multiple vibrational modes during wave propagation. This localization ensures that the vibrational energy of the knots does not dissipate as the deformation wave propagates, resulting in undamped propagation across the 5D brane, consistent with the conservation of mass and energy in the universe.

Physically, these knots arise at points where $\partial_{x^4}\Phi = 0$, indicating local maxima or minima in the deformation field. Their stability results from the effective potential $V(\Phi)$, which reaches a local minimum at these points. We describe these structures using the following effective Lagrangian on 4D slices:

$$\mathcal{L}_{slice} = -\frac{1}{2}h^{\mu\nu}\partial_\mu A(x^\mu)\partial_\nu A(x^\mu) - V(A(x^\mu)) \tag{5}$$

where $A(x) \equiv \Phi$ is the scalar field representing the amplitude of local microscopic deformation within the wave's crests and troughs. In these regions, the gradient $\partial_{x^4}V_\Phi$ vanishes, leading to near-zero effective gauge field mass and enabling stable interactions.

These deformation knots exhibit localized energy, stability, and particle-like properties in the 4D perspective, effectively behaving as matter particles. Analogous mechanisms are seen in solitonic models such as Q-balls and Skyrmions [16]; our model generalizes this concept to a higher-dimensional brane setting.

In our model, the deformation knots are not static field defects localized in the brane; instead, they are dynamically propagating maxima within the longitudinal wave packet along the fifth dimension x^4. Their stability is ensured not by topological protection, but by the robust form of the wave peak, which remains a local maximum under small perturbations during propagation. So the knot structures are stable in the sense that they ride on the crest and trough of the deformation wave, maintaining their peak amplitude as they move forward along x^4, thus not subject to local destabilization as in fixed-point configurations.

Hence, we propose that all ordinary matter—including baryons and Standard Model particles—arises as localized excitations within the membrane's geometric deformation. This unifies matter and spacetime structure within a single geometric framework, bridging membrane cosmology and particle physics.

Furthermore, this perspective is consistent with the idea of induced matter theory, which proposes that 4D matter arises from the geometry of higher-dimensional spacetime [17] [18]. However, our model goes further by offering a dynamical wave-based geometric mechanism for generating both matter and curvature.

The universe emerges as a wave crest or trough propagating along a higher-dimensional brane embedded in an extended bulk spacetime. All matter and energy in the universe come from the brane deformation, and the curvature of spacetime in the universe is equivalent to the brane deformation. Undamped propagation of brane deformation waves ensures the conservation of mass and energy in the universe.

Within the stable 4D slice spacetimes at wave crests and troughs, these deformation knots can act as secondary wave sources, emitting waves that exhibit diffraction and interference phenomena. These effects arise naturally from the wave-like nature of the knots' wave functions, potentially influencing the distribution of matter and energy in the 4D slices, which may leave observable imprints in the cosmic microwave background (CMB) anisotropies or large-scale structure formation.

The localized wave crests and troughs correspond to regions where Φ attains extreme values, forming self-sustaining solitonic structures that support stable gauge fields. These regions serve as the basis for two types of observable universes:

- Wave crest regions correspond to matter-dominated universes (like our own),
- Wave trough regions correspond to antimatter-dominated universes (antimatter counterparts that remain causally disconnected from our own).

The fluctuating inter-wave regions remain unstable and are identified with dark energy and dark matter domains.

2.3. Brane and Bulk Actions

2.3.1. Total Action

The total action S_{total} includes contributions from the 6D bulk, 5D brane, Gibbons-Hawking-York boundary terms, and the 4D slices [14]:

$$S_{total} = S_{bulk} + S_{brane} + S_{GHY} + \int_{slices} S_{slice} \tag{6}$$

2.3.2. 6D Bulk Action

The action for the 6D bulk spacetime (M^6) is given by [13]:

$$S_{bulk} = \int_{M^6} \mathrm{d}^6 x \sqrt{-g^{(6)}} \left[-\Lambda_6 \right] \tag{7}$$

where:

- Λ_6 : 6D cosmological constant;

Thus, the 6D bulk action assumes $g_{MN}^{(6)}$ as a fixed background geometry, such as Minkowski ($\Lambda_6 = 0$) or AdS ($\Lambda_6 < 0$), with gravitational dynamics confined to the brane.

2.3.3. 5D Brane Action

The action for the 5D brane embedded in the 6D bulk is [14]:

$$S_{brane} = \int_{M5} \mathrm{d}^5 x \sqrt{-g^{(5)}} \left(-\sigma + \mathcal{L}_{deform}^{(5)} \right) \tag{8}$$

where:

- σ : Brane tension;
- $\mathcal{L}_{deform}^{(5)}$: describes the dynamics of the deformation field Φ on the brane.

$$\mathcal{L}_{deform}^{(5)} = \frac{1}{2} g_{ab}^{(5)} \partial_a \Phi \partial_b \Phi - V(\Phi) \tag{9}$$

where Φ is a scalar field representing membrane deformations.

2.3.4. 4D Slice Action

In our model, the quantized deformation "knots" display quantized microscopic characteristics when they exist alone, but when they are gathered together, they display certain macroscopic characteristics. The emergence of gravity in 4D slice spacetimes—formed at the wave crests and troughs of the brane deformation wave—is not postulated but derived from a physical mechanism rooted in the brane's elastic dynamics. Specifically, as microscopic longitudinal deformations "knots" individual knots induce only small spacetime distortions, since the membrane is connected, this "knot" will also affect other points on the membrane, so their cumulative effect over large regions leads to measurable macroscopic spacetime bending of the brane within each stable slice region. This macroscopic bending, encoded geometrically as the Ricci scalar R of the induced 4D metric, serves as a geometric response balancing the internal tension generated by the cumulative microscopic longitudinal deformations "knots". So the gravity is not an external field added by hand, but a natural geometric consequence of the membrane's intrinsic deformation. Specifically, as the deformation wave propagates along the fifth spatial dimension, it accumulates and causes the membrane to bend, resulting in effective 4D curvature.

We propose the following relation as the physical basis for the emergence of gravity (The proof is in Appendix A):

$$\varepsilon_{\Phi}(x) = kR(x) \tag{10}$$

where

- $\varepsilon_{\Phi}(x)$: the local energy density of the deformation field at point x on the brane.
- $R(x)$: the local Ricci scalar curvature at point x on the brane.
- k: a proportionality constant.

This equation shows that the 4D curvature R arises naturally as a geometric response to the internal deformation stress. Unlike traditional brane-world models that derive Einstein equations via Gauss-Codazzi projections from 5D Einstein tensors [14] [19], our approach ties the curvature directly to the membrane's physical deformation dynamics.

Importantly, although Equation (10) differs in form from the traditional Einstein field equations (EFE), it encapsulates the same fundamental principle: that spacetime curvature is determined by the local distribution of matter and energy. This proportionality explicitly demonstrates, both mathematically and physically, that the energy density arising from deformation knots induces curvature in the 4D slices. In this sense, Equation (10) provides a concrete realization of the core idea behind the EFE-that matter tells spacetime how to curve-even though it arises here from the specific dynamics of brane deformations rather than being assumed as a geometric postulate.

Moreover, while the Einstein-Hilbert action postulates a Lagrangian density linear in the Ricci scalar R, it does not explain why matter and energy should generate curvature in this way. In contrast, Equation (10) suggests a possible physical interpretation for this proportionality, arising from the dynamics of deformation knots. Our model thus proposes that matter and energy arise as dynamical geometrical deformations of the brane, providing a physical mechanism that naturally links local energy densities to spacetime curvature and offering insight into how matter not only curves spacetime but also maintains stability through propagating deformation waves. Although this does not constitute a rigorous derivation of the Einstein-Hilbert action, it offers a complementary perspective on the physical origins of gravitational curvature.

To consistently encode this geometric response in the variational formulation, the gravitational Lagrangian density $\mathcal{L}_{grav}$ for each 4D slice must then include a term linear in R. This choice is not an arbitrary borrowing from General Relativity but arises naturally as the unique linear term consistent with (i) the observed curvature-force relation, (ii) general covariance, and (iii) the requirement that the resulting field equations remain second order.

In each localized 4D slice—formed at the crests and troughs of the membrane deformation wave—the total action is composed of a gravitational part and a deformation field part:

Total action;

$$S_{slice} = S_{grav} + S_{deform} \tag{11}$$

Gravitational action;

$$S_{grav} = \int d^4x\sqrt{-h}\,\mathcal{L}_{grav} = \int d^4x\sqrt{-h}\,\frac{1}{2\kappa_4}R \tag{12}$$

where $\kappa_4 = \frac{8\pi G}{c^4}$, $h = det\left(h_{\mu\nu}\right)$, and $R = h^{\mu\nu}R_{\mu\nu}$ is the 4D Ricci scalar constructed from the induced metric $h_{\mu\nu}$.

This is the Einstein-Hilbert action, indicating that the Einstein Field Equations emerge self-consistently from the wave-induced deformation of the membrane. Thus, gravity has a concrete geometric origin within this model, without relying on extrinsic assumptions or additional fields

Deformation field action:

$$S_{deform} = \int d^4x\sqrt{-h}\,\mathcal{L}_{slice} \tag{13}$$

where:

- $\mathcal{L}_{slice}$: Lagrangian density for the slice14. It includes: Gauge field terms describing the electromagnetic, weak, and strong interactions from 4D projections; matter terms representing stable deformation “knots.”

The deformation Lagrangian density is expressed as Equation (5): The potential term $V\left(A\left(x^{\mu}\right)\right)$ encodes effective interactions or energy density associated with the deformation modes. The Ricci scalar R captures the intrinsic curvature of the 4D slice, which arises as a macroscopic geometric response to the accumulation and coherence of microscopic deformation waves propagating along the fifth spatial direction.

2.4. Stability and Localization of Gauge Fields

Unlike conventional brane-world models where fields are assumed to be confined by postulated mechanisms, in our framework the stability of gauge fields naturally emerges due to the structure of the deformation potential. The gauge field energy density is tightly correlated with the spatial gradient of the deformation potential:

$$V_{gauge} = \lambda \left(\frac{\partial V_{\Phi}}{\partial x^4} \right)^2 \tag{14}$$

where:

- $\lambda > 0$ is a coupling constant that determines the interaction strength.
- x^4 is the deformation wave's propagation direction.
- V_{Φ} is the brane's deformation potential [20].

This formulation ensures that gauge fields are only stable in wave crest and trough regions, while in inter-wave zones, where $\frac{\partial V_{\Phi}}{\partial x^4} \neq 0$, the gauge fields decay, preventing the formation of localized matter.

The specific form of the brane potential V_{Φ} remains to be determined, with its parameters intended to be constrained by observational data.

2.5. Effective Mass

In our model, the gauge field excitations acquire an effective mass that depends on the spatial structure of the brane's deformation potential. Instead of reconstructing a full interaction Lagrangian between the gauge field A_M and the deformation field Φ, we directly postulate an effective mass term based on physical intuition. Specifically, we assume that the squared effective mass is induced by the spatial gradient of the deformation potential $V_{brane}(\Phi)$ along the propagation direction x^4 [20]:

$$\mathcal{M}_{eff}^2(\Phi) = -\lambda \left(\frac{\partial V_{\Phi}}{\partial x^4} \right)^2 \tag{15}$$

where:

- $\mathcal{M}_{eff}^2(\Phi)$ represents the squared effective mass of gauge bosons [21].
- The negative correlation ensures that gauge bosons remain massless or near-massless in wave crest and trough regions, allowing standard model interactions to persist [22]. And induce tachyonic instability in dark sectors enabling exponential growth of perturbations that lead to energy storms, while ensuring stability at crests and troughs.

This construction captures the core physical mechanism: at wave crests and troughs where the potential reaches extrema, the spatial gradient vanishes and gauge fields become massless, allowing for stable propagation. In contrast, in inter-wave regions where the deformation gradient is significant, the induced negative mass squared leads to tachyonic instabilities. Although this effective mass is not derived from a full five-dimensional action, it reflects a physically motivated structure commonly used in effective field theories and topological soliton models. This formulation allows us to analyze field stability without introducing additional coupling terms in the brane action.

Although the interaction does not appear as an explicit cross term in the Lagrangian, the gauge field mass arises directly from the deformation field profile via Equation (15). This establishes a geometry-induced coupling, where the brane deformation determines gauge field dynamics. Similar mechanisms appear in domain-wall localization and Kaluza-Klein [17] inspired models.

This implies that wave crest and trough regions maintain nearly massless gauge bosons, enabling standard model physics, whereas in inter-wave regions, the effective mass becomes nonzero, inhibiting matter formation.

For simplicity, we assume that all gauge fields share the same effective mass, as their stability is primarily determined by the geometric deformation of the brane. Future work will explore the impact of distinct effective masses for different gauge fields to account for their physical differences.

3. Results and Discussion

3.1. The Transition from a Membrane Deformation Field to Inflationary Dynamics and the Formation of "Universe Factory"

In this section, we explore how the previously introduced membrane deformation field (Φ) transitions into inflationary dynamics and subsequently leads to the formation of "Universe Factory"—mechanisms that continuously generate new observable universes through deformation wave ripples. This process is delineated through a series of detailed theoretical derivations and physical explanations. We delineate this process into three distinct evolutionary stages, analogous yet distinct from the standard cosmological paradigm: the inflation zone stage, the transition stage, and the membrane oscillation-dominated stage. These stages are driven by the interplay between external energy input and the intrinsic properties of the five-dimensional (5D) brane, offering a novel framework that aligns with key observational constraints, such as the Cosmic Microwave Background (CMB) power spectrum, while extending beyond the conventional ΛCDM model. We provide detailed theoretical derivations, physical explanations, and comparisons with standard cosmology to substantiate this model.

3.1.1. Inflation Zone Stage: High-Energy Gaussian Perturbations and Extended Inflationary Dynamics

The initial stage of our model, termed the inflation zone stage, corresponds broadly to the radiation-dominated era of standard cosmology but encompasses a significantly extended inflationary period driven by high-energy Gaussian perturbations. These perturbations, arising from random energy impacts within the 6D bulk spacetime, inject a sudden influx of kinetic energy into the 5D brane, initiating a rapid deformation that propagates as a shock wave. The radial extent of the Gaussian perturbation is limited to $R_0 = 10^{-12}$ meters and the temporal profile of the energy is modeled as:

$$E_t = E_0 e^{-\frac{t^2}{2\tau^2}} \tag{16}$$

where:

- E_0: total energy of the Gaussian perturbation.
- E_t: remaining energy at time t.
- τ: characteristic timescale of the perturbation.

Such an extremely energetic perturbation inevitably generates a deformation shock wave. Assuming the medium has a strong restoring force (analogous to a stiff membrane) and the medium's density ρ has a wide linear response range to external force, we use the Hugoniot equation of linear shock propagation to describe the velocity of the shock front:

$$V_s = \frac{\eta}{\eta - 1} u_\Phi \tag{17}$$

where:

- η: compression ratio ρ/ρ_0.
- u_Φ: deformation velocity of the membrane material point.

If the radius of the Gaussian energy disturbance is R_0, according to the above formula, the radius of the shock wave caused by it is $\frac{\eta R_0}{\eta - 1}$, and the volume of the sphere in the four-dimensional space on the membrane is $\frac{\pi^2}{2}\left(\frac{\eta R_0}{\eta - 1}\right)^4$, Due to the high rigidity of the membrane, it can be assumed that ρ is approximately a constant, and applying Newton's second law and energy loss formula $-\mathrm{d}E = F\mathrm{d}x$, one arrives at:

$$F = m\dot{u}_\Phi = \rho\left(\frac{\pi^2}{2}\left(\frac{\eta R_0}{\eta - 1}\right)^4\right)\dot{u}_\Phi = -\frac{\frac{\mathrm{d}E_t}{\mathrm{d}t}}{\frac{\mathrm{d}x}{\mathrm{d}t}} = -\frac{\frac{\mathrm{d}E_t}{\mathrm{d}t}}{u_\Phi} \tag{18}$$

$$\dot{u}_\Phi u_\Phi = -\frac{2\frac{\mathrm{d}E_t}{\mathrm{d}t}}{\rho\pi^2\left(\frac{\eta R_0}{\eta - 1}\right)^4} = \frac{\mathrm{d}u_\Phi^2}{\mathrm{d}t} \tag{19}$$

$$u_\Phi^2 = \frac{4}{\rho\pi^2\left(\frac{\eta R_0}{\eta - 1}\right)^4}\left(E_0 - E_t\right) \tag{20}$$

$$u_\Phi = \left(\frac{4}{\rho\pi^2\left(\frac{\eta R_0}{\eta - 1}\right)^4}\left(E_0 - E_t\right)\right)^{\frac{1}{2}} = \frac{2}{\pi\left(\frac{\eta R_0}{\eta - 1}\right)^2}\rho^{-\frac{1}{2}}\left(E_0 - E_t\right)^{\frac{1}{2}} \tag{21}$$

$$V_s = \frac{\eta}{\eta - 1}u_\Phi = \frac{\eta - 1}{\eta}\frac{2}{\pi R_0^2}\rho^{-\frac{1}{2}}\left(E_0 - E_t\right)^{\frac{1}{2}} = \frac{\eta - 1}{\eta}\frac{2}{\pi R_0^2}\left(\frac{E_0}{\rho}\right)^{\frac{1}{2}}\left(1 - e^{-\frac{t^2}{2\tau^2}}\right)^{\frac{1}{2}} \tag{22}$$

Assuming the radial scale of the inflation zone is $R(t)$, then:

$$\dot{R}(t)=V_s=\frac{\eta-1}{\eta}\frac{2}{\pi R_0^2}\left(\frac{E_0}{\rho}\right)^{\frac{1}{2}}\left(1-\mathrm{e}^{-\frac{t^2}{2\tau^2}}\right)^{\frac{1}{2}} \tag{23}$$

$$\ddot{R}(t)=\frac{\eta-1}{\eta}\frac{2}{\pi R_0^2}\left(\frac{E_0}{\rho}\right)^{\frac{1}{2}}\frac{t\mathrm{e}^{-\frac{t^2}{2\tau^2}}}{\tau^2\left(1-\mathrm{e}^{-\frac{t^2}{2\tau^2}}\right)^{\frac{1}{2}}} \tag{24}$$

$$R(t)=\int_0^t\dot{R}(t')\mathrm{d}t'=\frac{\eta-1}{\eta}\frac{2}{\pi R_0^2}\left(\frac{E_0}{\rho}\right)^{\frac{1}{2}}\int_0^t\left(1-\mathrm{e}^{-\frac{t'^2}{2\tau^2}}\right)^{\frac{1}{2}}\mathrm{d}t' \tag{25}$$

$$\begin{aligned}\epsilon(t)&=1-\frac{\ddot{R}(t)R(t)}{\dot{R}(t)^2}\\&=1-\frac{\frac{\eta-1}{\eta}\frac{2}{\pi R_0^2}\left(\frac{E_0}{\rho}\right)^{\frac{1}{2}}\frac{t\mathrm{e}^{-\frac{t^2}{2\tau^2}}}{\tau^2\left(1-\mathrm{e}^{-\frac{t^2}{2\tau^2}}\right)^{\frac{1}{2}}}}{\left(\frac{\eta-1}{\eta}\frac{2}{\pi R_0^2}\left(\frac{E_0}{\rho}\right)^{\frac{1}{2}}\left(1-\mathrm{e}^{-\frac{t^2}{2\tau^2}}\right)^{\frac{1}{2}}\right)^2}\cdot\frac{\eta-1}{\eta}\frac{2}{\pi R_0^2}\left(\frac{E_0}{\rho}\right)^{\frac{1}{2}}\int_0^t\left(1-\mathrm{e}^{-\frac{t'^2}{2\tau^2}}\right)^{\frac{1}{2}}\mathrm{d}t'\\&=1-\frac{t\mathrm{e}^{-\frac{t^2}{2\tau^2}}}{\tau^2\left(1-\mathrm{e}^{-\frac{t^2}{2\tau^2}}\right)^{\frac{3}{2}}}\cdot\int_0^t\left(1-\mathrm{e}^{-\frac{t'^2}{2\tau^2}}\right)^{\frac{1}{2}}\mathrm{d}t'\end{aligned} \tag{26}$$

where:

- $\epsilon(t)$ is the slow-roll epsilon.

Let $C=\frac{\eta-1}{\eta}\frac{2}{\pi R_0^2}\left(\frac{E_0}{\rho}\right)^{\frac{1}{2}}$ equal 2.05×10^{47}, and let the characteristic time scale be $\tau=1.78\times10^{-32}$ seconds, according to the calculation (The Python calculation and plotting code is provided in Appendix B): within the interval 0 - 10^{-32} seconds, the function $R(t)$ increases from 10^{-12} meters to approximately 3.99×10^{14} meters. The expansion factor of this inflationary region is 3.99×10^{26}. This matches the inflationary expansion factor generally assumed by standard cosmology. During most of this inflationary period, the parameter $\epsilon(t)\ll1$, which satisfies the slow-roll condition. And it is a single-field inflation, the energy is also high. Therefore, the scalar spectral index: $n_s(t)\approx1-2\epsilon(t)$ [23], remains close to 1 throughout this phase. The average value of $n_s(t)$ is approximately 0.9607, aligning closely with the scalar spectral index inferred from cosmic microwave background observations.

As the shock wave expands, the energy of the Gaussian perturbation is rapidly depleted. The expansion velocity $\dot{R}(t)$ and acceleration $\ddot{R}(t)$ decline sharply. This causes the slow-roll parameter $\epsilon(t)$ to increase rapidly at the end of inflation, leading to a strong negative drift in the scalar spectral index $n_s(t)$, which can approach −1 after inflation concludes.

If the total perturbation energy is taken as $E_0 = 1.86 \times 10^{82}$ joules, this exceeds the total energy of the observable universe by a factor of approximately 6.6×10^{10}, this is sufficient to maintain the mass-energy density of the entire 5D propagation region of the deformation wave and generate several peak and trough universes therein. Despite the massive total energy, the peak energy density still remains several orders of magnitude below the Planck limit, so energy conservation is not violated during inflation.

This model thus offers an inflationary scenario in which energy originates from a Gaussian perturbation rather than from a vacuum expectation value. The model represents a "hot inflation" in which no reheating phase is needed. That is, radiation and relativistic particles exist throughout the inflationary process. However, before the peaks and troughs are generated, due to the instability of the gauge field, these radiation and relativistic particles must be quickly stabilized in the stable gauge field of the 4D slice space-time region of the peaks and troughs that appear later, and then they can combine to form protons and neutrons after gaining mass. When the energy density is further reduced, nuclear synthesis also occurs synchronously in this region. More detailed quantitative research will be carried out in the next step.

The inflation zone stage consists of two subphases:

- Gaussian Perturbation Phase: A brief initial period during which the random energy impact (often appears in bulk spacetime) from bulk spacetime triggers the deformation wave Φ, analogous to the standard inflationary epoch driven by a scalar field [6]. This phase generates the primordial perturbations necessary for structure formation.
- External Energy-Dominated Phase: After the Gaussian perturbation ceases, the residual external energy continues to drive the deformation wave's propagation, extending the inflationary period significantly. The inflation zone expands as the wave propagates, producing wave crests and troughs that eventually detach as independent universes.

This extended inflation ensures the isotropy observed in our universe, a 4D slice along the tangential direction of the 5D deformation wave. The prolonged expansion smooths out tangential variations, consistent with the CMB's high degree of uniformity ($\frac{\Delta T}{T} \sim 10^{-5}$) [7]. The standard inflationary phase is thus a small subset of this stage, occurring during the Gaussian perturbation phase, while the subsequent external energy-driven expansion amplifies the spatial and temporal scales of the "universe factory".

3.1.2. Transition Stage: The Shock Wave Energy Conversion and Deceleration

The second stage, the transition stage, corresponds to the matter-dominated era in standard cosmology, where the universe's expansion decelerates ($a \sim t^{\frac{2}{3}}$) due to the dominance of matter density ($\rho_m \propto a^{-3}$) [10]. In our model, this stage marks the gradual conversion of the shock wave energy residual from the inflation zone into the membrane's intrinsic oscillation energy. The wave speed remains faster than the membrane's natural propagation speed ($V_T > C_{brane}$), but it decelerates as the shock wave energy dissipates:

$$V_T(t) = \sqrt{\frac{T + E_{s0}e^{-\gamma t} - V_{gravity}(t)}{\rho}} \tag{27}$$

where:

- $V_T(t)$ is the wave speed in transition stage.
- E_{s0} is the residual shock wave energy in the start of the transition stage.
- T is the brane's bulk modulus.
- γ is the transition coefficient.
- $V_{gravity}(t)$ is the gravitational potential.

The deformation wave equation governs this transition:

$$-\frac{1}{\sqrt{-g}}\partial_\mu\left(\sqrt{-g}g^{\mu\nu}\partial_\nu\Phi\right) + \frac{\partial V_\Phi}{\partial\Phi} = 0 \tag{28}$$

with the shock wave energy term $E_{S0}e^{-\gamma t}$ diminishing over time.

During this stage, the wave crests and troughs—representing matter and antimatter-dominated universes—continue to form and detach from the inflation zone, while the expansion rate slows. This mirrors the standard model's matter dominated phase, where gravitational clustering begins, but in our framework, the deceleration reflects the waning influence of external energy rather than a shift in energy density components. The transition stage ends when the external energy is fully converted, and the membrane's intrinsic oscillations take over.

3.1.3. Membrane Oscillation-Dominated Stage: Intrinsic Dynamics and Acceleration

The third stage, the membrane oscillation-dominated stage, aligns with the dark energy-dominated era of standard cosmology, characterized by accelerated expansion ($a \propto e^{Ht}$) driven by a cosmological constant or dark energy ($\Omega_\Lambda = 0.7$) [7]. In our model, this stage begins when the membrane's intrinsic oscillation energy dominates, with the wave speed $V_m(t)$ governed by:

$$V_m(t) = \sqrt{\frac{T - V_{gravity}(t)}{\rho}} \tag{29}$$

where is the gravitational potential induced by the deformation's energy-momentum tensor. Initially, $V_m(t) < C_{brane}$, due to gravitational binding from the matter density within wave crests and troughs. As the deformation wave propagates and the spatial extent increases, the matter density dilutes ($\rho_m \propto a^{-3}$), reducing

$V_{gravity}$, and the wave speed accelerates, approaching:

$$C_{brane} = \sqrt{\frac{T}{\rho}} \tag{30}$$

So in the third stage, the accelerated expansion typically attributed to dark energy in standard cosmology arises from the dynamics of the deformation wave Φ along the 5D brane. The wave's intrinsic speed C_{brane} representing its propagation across the entire 5D spacetime (4 spatial dimensions), is a stable property determined by the brane's bulk modulus T (units: $J \cdot m^{-4}$) and brane bulk density ρ (units: $J \cdot m^{-6} \cdot s^{-2}$). In natural units ($c = 1$), T units: GeV^5 and ρ units: GeV^5.

The brane bulk modulus T and brane bulk density ρ are fundamental parameters of the 5D brane, determining the wave speed C_{brane} that reflects its elastic dynamics.

When gravitational potential energy becomes negligible, the wave front propagation distance in our model is defined as

$$R(t) = R_{n0} + C_{brane}(t - t_{n0}) \tag{31}$$

where:

- R_{n0} is the initial wavefront distance at time t_{n0}.
- C_{brane} is the wave speed on the membrane.
- t_{n0} marks the onset of this regime.

The Hubble parameter is:

$$H = \frac{\dot{a}}{a} = \frac{\partial_t R(t)}{R(t)} \tag{32}$$

This reflects the synchronous expansion of wave crests and troughs with the wavefront distance *R*, aligning with the expansion behavior of the 4D cosmological scale factor $a(t)$.

In the standard ΛCDM model, when gravitational potential energy is negligible (i.e., matter and radiation densities approach zero), the Hubble parameter is dominated by dark energy, satisfying:

$$H^2 = \frac{\Lambda c^2}{3} \tag{33}$$

where Λ is the cosmological constant and c is the speed of light. The dark energy density ρ_{DE} relates to Λ via $\rho_{DE} = \frac{\Lambda c^2}{8\pi G}$. To connect our model with standard cosmology, we assume the initial moment ($t = t_{n0}$) when gravitational potential energy becomes negligible:

$$R(t_{n0}) = R_{n0} \tag{34}$$

$$\partial_t R(t)\big|_{t=t_{n0}} = C_{brane} \tag{35}$$

$$H = \frac{\partial_t R(t)}{R(t)} = \frac{C_{brane}}{R_0} \tag{36}$$

Comparing this with the ΛCDM expression for the dark energy-dominated phase:

$$H^2 = \frac{\Lambda c^2}{3} = \frac{C_{brane}^2}{R_0^2} \tag{37}$$

Solving for Λ:

$$\Lambda = \frac{3C_{brane}^2}{c^2 R_{n0}^2} = \frac{3T}{c^2 R_{n0}^2 \rho} \tag{38}$$

$$\rho_{DE} = \frac{\Lambda c^2}{8\pi G} = \frac{3T}{8\pi G R_{n0}^2 \rho} \tag{39}$$

These expressions indicate that both Λ and ρ_{DE} depend on the brane's bulk modulus T, brane bulk density ρ and the initial wave front distance when gravitational potential energy becomes negligible R_{n0}.

In future work, their values will be constrained to align the projected 4D density with the observed dark energy density $\rho_{DE} \approx 7\times10^{-27}\ \text{kg/m}^3$, yielding a pressure $P_{DE} = \rho_{DE}$ consistent with the equation of state [7]. This framework ties the stable, long-term expansion of our universe to the 5D brane's intrinsic properties, distinct from short-lived phases, offering a physical basis for dark energy without ad hoc fields.

Our three-stage framework-spanning the inflation zone, transition, and membrane oscillation-dominated stages-offers a coherent alternative to standard cosmology. It aligns with CMB observations, producing a near-scale-invariant spectrum ($n_s \approx 0.96$) through an inflationary mechanism, while providing a unified explanation for universe formation, deceleration, late-time acceleration and dark energy mechanism within the deformation wave paradigm [14] [24].

3.2. The Stability Conditions for Gauge Fields at Wave Crests and Troughs

In this section, we rigorously derive the stability conditions for gauge fields localized at the wave crests and troughs of the membrane deformation field Φ. We demonstrate that gauge fields are stable only in regions where the deformation field's potential energy $V_{brane}(\Phi)$ reaches extrema (absolute maxima) and the deformation field's kinetic energy vanishes. Furthermore, wave crests are interpreted as matter-dominated universes, wave troughs as antimatter-dominated universes, and their annihilation is explained geometrically as the cancellation of deformation "knots."

3.2.1. Basic Settings and Equations

Gauge Field Settings:

The gauge fields are set as [20]:

$$U(1)\times SU(2)\times SU(3)\times U(1)'\times B_{\mu\nu}\times C_{d\nu\rho} \tag{40}$$

where:

- The electromagnetic force A_μ is governed by the $U(1)$ group.
- The weak interaction W_μ^a is governed by the $SU(2)$ group.
- The strong force G_μ^a is governed by the $SU(3)$ group.

The additional gauge fields are induced by the geometric deformation of the brane:

- The $U(1)'$ gauge field X_μ is induced by brane deformation.
- The $B_{\mu\nu}$ 2-form field is induced by the topological solitons of the brane.
- The $C_{d\nu\rho}$ 3-form field is induced by the Chern-Simons action.

Total System Action:

$$S=\int d^5x\sqrt{-g_{MN}}\left(-\frac{1}{4}F_{MN}F^{MN}+\frac{1}{2}\mathcal{M}_{eff}^2(\Phi)A_MA^M+\frac{1}{2}\partial_M\Phi\partial^M\Phi\right.$$
$$\left.-V(\Phi)-\frac{1}{4}X_{MN}X^{MN}-\frac{1}{12}H_{MNP}H^{MNP}-\frac{1}{48}G_{MNPQ}G^{MNPQ}\right) \tag{41}$$

where:

- g_{MN} is the 5-dimensional spacetime metric ($M,N=0,1,2,3,4$).
- $F_{MN}=\partial_MA_N-\partial_NA_M$ is the gauge field strength tensor.
- $X_{MN}=\partial_MX_N-\partial_NX_M$ is the additional $U(1)$'gauge field.
- $H_{MNP}=\partial_MB_{NP}+\partial_NB_{PM}+\partial_PB_{MN}$ is the geometrically induced 2-form field.
- $G_{MNPQ}=\partial_MC_{\nu\rho\sigma}+\partial_\nu G_{\rho\sigma\mu}+\partial_\rho G_{\sigma\mu\nu}$ is the Chern-Simons 3-form field.
- A_M is the gauge field potential.
- Φ is the deformation field.
- V_{brane} is the deformation field potential, taking maximum values at wave crests and troughs, zero at $\Phi=0$, and satisfying $\frac{\partial^2V_{brane}}{\partial\Phi^2}>0$ (elastic stability).
- $\mathcal{M}_{eff}^2(\Phi)$ is the effective mass of the gauge field.

Effective Mass Definition as Equation (15):

The negative sign is chosen to induce tachyonic instability in dark sectors enabling exponential growth of perturbations that lead to energy storms, while ensuring stability at crests and troughs.

Gauge Field Potential Function:

The gauge field potential function is:

$$V_{gauge}=\lambda\left(\frac{\partial V_\Phi}{\partial x^4}\right)^2 \tag{42}$$

which forms a potential well at the wave crests and troughs ($\frac{\partial V_\Phi}{\partial x^4}=0$).

Field Equations:

Gauge Field Equation:

$$\frac{1}{\sqrt{-g}}\partial_N\left(\sqrt{-g}F^{MN}\right)+\frac{1}{2}\mathcal{M}_{eff}^2(\Phi)A^M=0 \tag{43}$$

Deformation Field Equation:

$$\frac{1}{\sqrt{-g}}\partial_N\left(\sqrt{-g}F^{MN}\right)-\frac{\partial V_{brane}}{\partial\Phi}+\frac{1}{2}\frac{\partial\mathcal{M}_{eff}^2(\Phi)}{\partial\Phi}A_MA^M=0 \tag{44}$$

3.2.2. Stability Proof in Wave Crest and Trough Regions

To derive the behavior of gauge field perturbations in the wave crest and trough regions, we begin with the linearized field equation. Since the deformation potential reaches an extremum in these regions, its spatial gradient vanishes, and thus:

$$\mathcal{M}_{eff}^2(\Phi) = -\lambda\left(\frac{\partial V_\phi}{\partial x^4}\right)^2 = 0 \tag{45}$$

The gauge field satisfies the free-field equation:

$$\nabla^N F_{NM} = 0 \tag{46}$$

Under the Lorenz gauge condition $\nabla^M A_M = 0$, we substitute $F_{NM} = \partial_N A_M - \partial_M A_N$ and obtain:

$$\Box A_M = 0 \tag{47}$$

We now solve this wave equation. In locally flat coordinates (t, x^1, x^2, x^3, x^4), the d'Alembertian becomes:

$$\Box A_M = \eta^{PQ}\partial_P\partial_Q A_M = -\partial_t^2 A_M + \sum_{i=1}^{4}\partial_i^2 A_M \tag{48}$$

We assume a separable plane-wave solution:

$$A_M(x) = \epsilon_M \mathrm{e}^{ik_N x^N} \tag{49}$$

Substituting into the wave equation gives:

$$A_M = k_N x^N \epsilon_M \mathrm{e}^{ik_N x^N} = 0 \Rightarrow k_N x^N = 0 \tag{50}$$

Thus, the solution describes a massless plane wave satisfying:

$$A_M(x) = \epsilon_M \mathrm{e}^{ik_N x^N}, \quad k_N x^N = 0 \tag{51}$$

This solution is oscillatory and does not grow with time, indicating the field is linearly stable in wave crest and trough regions.

Energy Analysis:

Perturbation energy density:

$$\varepsilon = \frac{1}{2}\left[\left|\partial_t \delta A_M\right|^2 + \left|\nabla \delta A_M\right|^2\right] \tag{52}$$

Due to energy conservation, the system is stable against perturbations. The law of energy conservation ensures that even in the presence of perturbations in the wave crest and trough regions, the total energy of the system does not change without limit, thus maintaining the stability of the gauge field.

3.2.3. Proof of Instability Far from Wave Crests and Troughs

Effective Mass Analysis:

In regions far from wave crests and troughs, the deformation potential varies significantly, and the induced effective mass becomes negative:

$$\left|\frac{\partial V_{brane}}{\partial x^4}\right| \gg 0 \tag{53}$$

$$\mathcal{M}_{eff}^{2}(\Phi) \ll 0 \tag{54}$$

The linearized equation becomes:

$$\Box \delta A_M = M_{eff}^{2}(\Phi) \delta A_M \tag{55}$$

Define $\mu^2 \equiv -M_{eff}^{2}(\Phi) > 0$, then:

$$\Box \delta A_M = -\mu^2 \delta A_M \tag{56}$$

In locally flat coordinates, this reads:

$$-\partial_t^2 \delta A_M + \nabla^2 \delta A_M = -\mu^2 \delta A_M \Rightarrow \partial_t^2 \delta A_M = \nabla^2 \delta A_M + \mu^2 \delta A_M \tag{57}$$

Assume a separable solution:

$$A_M(x) = \epsilon_M \mathrm{e}^{ik_N x^N} \tag{58}$$

We work in a locally flat coordinate system where $x^N = (t, x)$, and accordingly decompose the momentum as $k^N = (\omega, k)$.

Substituting yields:

$$\omega^2 = \mu^2 - |k|^2 \tag{59}$$

Hence, for low spatial wave number $|k|^2 < \mu^2$, we obtain exponential growth:

$$\delta A_M(t) \sim \mathrm{e}^{\gamma t}, \gamma = \sqrt{\mu^2 - |k|^2} \tag{60}$$

This means that in areas far from the wave crests and troughs, the effective mass of the gauge field becomes a large negative value, in sharp contrast to the zero effective mass at the wave crests and troughs. This large negative effective mass will lead to the instability of the system 20.

In the long-wavelength limit $|k| \to 0$, we have:

$$\gamma \approx \sqrt{\left|M_{eff}^{2}(\Phi)\right|} \tag{61}$$

Due to large $\left|\mathcal{M}_{eff}^{2}(\Phi)\right|$, tachyonic modes grow rapidly. The exponential growth mode indicates that the perturbation will increase rapidly with time, destroying the stability of the system. The growth time scale $\tau \sim 1/\gamma$ is very short. This means that the perturbation will change significantly in a very short time, making it difficult for the system to maintain a stable state. It leads to rapid gauge field collapse. Eventually, the gauge field cannot stably exist in the region far from the wave crests and troughs.

Energy Storm:

Violent tachyonic modes lead to:

- Rapid changes in gauge field energy density. The rapid change in energy density reflects the unstable state of the system, and the energy is no longer in a relatively stable distribution.
- Violent local energy fluctuations. In the local region of space, there are violent fluctuations and changes in energy, further exacerbating the instability of the system.
- Formation of persistent energy storms. The entire region is in a state of con-

tinuous violent energy changes, like a storm, making it impossible for the gauge field to form a stable structure in this region.

- Energy storms, driven by tachyonic modes ($\mathcal{M}_{eff}^2(\Phi) < 0$), disrupt small-scale spacetime curvature traces (e.g., stellar scales) in dark sectors, preventing observable dark matter effects at these scales, while galaxy-scale traces persist as the source of dark matter gravity.

3.2.4. Proof of Barrier Effect near Wave Crests and Troughs

Effective Mass Asymptotic Behavior:

At distance δx^4 from wave crest/trough points:

$$\mathcal{M}_{eff}^2(\Phi) = -\lambda \left(\left. \frac{\partial^2 V_{brane}}{\partial (x^4)^2} \right|_{x_0^4} \right)^2 (\delta x^4)^2 + O\left((\delta x^4)^3 \right) \tag{62}$$

This equation gives the asymptotic expression of the effective mass of the gauge field in the region near the wave crest and trough. It shows that the effective mass is related to the distance from the wave crest and trough points and that the absolute value of the effective mass is relatively small in the nearby region.

Slow Region Barrier:

In the nearby regions:

- $\left|\mathcal{M}_{eff}^2(\Phi)\right|$ is very small. In contrast to the large negative effective mass in the region far from the wave crests and troughs, the properties of the nearby region are very different.
- The perturbation growth rate $\gamma = \sqrt{\left|\mathcal{M}_{eff}^2(\Phi)\right|}$ is small. This means that the growth rate of the perturbation in the nearby region is very slow and will not grow rapidly like in the far region, leading to system collapse.
- The growth time scale $\tau \sim 1/\gamma$ is very long. This indicates that the perturbation needs a long time to reach a significant level, which provides a certain protective effect for the wave crest and trough regions.

Quantum Tunneling Effect Shielding:

Since $V_{gauge} = \lambda \left(\frac{\partial V_\phi}{\partial x^4} \right)^2$ forms a deep potential well at the wave crests and troughs, the tunneling probability approaches zero, ensuring the stability of the gauge field.

For further analysis of the quantum tunneling probability [25]:

$$P_{tunnel} \propto \exp\left(-\frac{2}{\hbar} \int \sqrt{2m\left(E - V_{gauge}\right)} \mathrm{d}x \right) \tag{63}$$

Because the potential well formed by $V_{gauge} = \lambda \left(\frac{\partial V_\phi}{\partial x^4} \right)^2$ is extremely deep at the wave crests and troughs, the tunneling probability decays exponentially and is almost zero, strictly confining the gauge field to the wave crest and trough regions.

Localization Proof:

The localization of the gauge field in the wave crest/trough region is protected because:

- Internal perturbations are stable ($\mathcal{M}_{eff}^2(\Phi)=0$). The stability of the gauge field itself at the wave crest and trough is the basis of localization.
- Nearby regions form a slow-growth barrier. The slow-growth barrier in the nearby region slows down the propagation of external perturbations to the wave crest and trough regions and plays a role of isolation and protection.
- V_{gauge} forms quantum tunneling effect shielding by a deep potential well at the wave crests and troughs, the tunneling probability decays exponentially and is almost zero, strictly confining the gauge field to the wave crest and trough regions.
- External tachyonic modes cannot penetrate the slow region. This ensures that external unstable factors do not affect the stability of the wave crest and trough regions.
- Energy storms are effectively blocked. This makes the wave crest and trough regions free from the interference of external energy storms and maintains the stable state of localization.

Topological Irrelevance:

Due to the slow region barrier:

- The gauge field cannot propagate to distant regions. This limits the propagation range of the gauge field in space and ensures its locality in the wave crest and trough regions and nearby regions.
- Distant topological structures cannot affect the wave crest and trough regions. This shows that the stability and localization properties of the wave crest and trough regions are not affected by the complex topological structures in the distance and have relative independence.
- Boundary conditions do not influence localization properties. This further emphasizes the stability of the localization of the wave crest and trough regions and is not affected by external boundary conditions.

3.2.5. Conclusions

Wave Crest and Trough Regions:

- Zero effective mass. This is an important characteristic of this region, determining the special dynamic behavior of the gauge field in this region.
- The gauge field is stable against perturbations. It can maintain a stable state at the wave crest and trough and is not affected by small perturbations.
- Form stable 4D slices. In this region, the gauge field forms a relatively independent and stable 4-dimensional spacetime structure.

Distant Regions:

- Large negative effective mass leads to tachyonic modes. This makes the gauge field in the region far from the wave crests and troughs unstable, with rapidly growing perturbations.
- Form persistent energy storms. The entire region has violent energy fluctuations and cannot maintain a stable gauge field structure.

- Cannot affect wave crest/trough regions. Due to the barrier effect of the nearby region, the unstable factors in the distant region are effectively isolated.

Nearby Regions:

- Small negative effective mass forms a barrier. The special property of the effective mass in the nearby region provides protection for the wave crest and trough regions.
- Protects wave crest/trough regions. Prevents the intrusion of external unstable factors and maintains the stability of the wave crest and trough regions.
- Achieves "safe harbor" effect. Makes the wave crest and trough regions a relatively stable region, like a safe harbor in an energy storm.

The detailed mathematical description of stable deformation knots, including their quantization, wave function forms, and interactions, will be addressed in subsequent studies. Future work will focus on deriving the quantum field theory framework for these knots, their correspondence to gauge fields, and their potential observational signatures in the CMB or large-scale structure.

3.3. The Derivation of the Effective Gravitational Field Equations

This section derives the effective gravitational field equations on in the 4D wave crest and trough slice spacetimes within our deformation wave model. In 2.3.4, we propose that gravity emerges directly from a physical mechanism rooted in the brane's elastic dynamics and the expression of gravitational action is obtained. In the section, starting from the gravitational and the deformation wave's action, which is a purely geometric construct, we employ variational principles to systematically derive the EFE. The resulting energy-momentum tensor arises solely from the deformation wave's action, reflecting the brane's intrinsic dynamics, and incorporates contributions from matter, dark matter, and dark energy. These equations align with cosmological observations, such as the CMB scalar spectral index ($n_s \approx 0.96$) [7], galactic dark matter ratios ($\frac{\rho_{DM}}{\rho_b} \approx 5$) [10], and dark energy density ($\Omega_\Lambda \approx 0.7$) [11], while providing a physical mechanism for spacetime curvature, addressing a fundamental gap in General Relativity (GR).

3.3.1. Variational Derivation of the EFE

In 2.3.4, we obtain the Gravitational action in Equation (12) and total action in Equation (13).

In our deformation wave model, the gravitational action is mathematically and physically identical to the Einstein-Hilbert action S_{EH} in General Relativity (GR):

$$S_{EH} = \int \mathrm{d}^4 x \sqrt{-g} \frac{1}{2\kappa_4} R \tag{64}$$

with $h_{\mu\nu}$ replacing $g_{\mu\nu}$. As established in standard GR, the variation of this action with respect to the metric $h_{\mu\nu}$, incorporating the Gibbons-Hawking-York (GHY) boundary term to ensure a well-posed variational principle, yields:

$$\begin{aligned}\delta S_{grav} &= \int \frac{1}{2\kappa_4}\left(R_{\mu\nu} - \frac{1}{2}h_{\mu\nu}R\right)\delta h^{\mu\nu}\sqrt{-h}\,\mathrm{d}^4x \\ &= \int \frac{c^4}{16\pi G}\left(R_{\mu\nu} - \frac{1}{2}h_{\mu\nu}R\right)\delta h^{\mu\nu}\sqrt{-h}\,\mathrm{d}^4x\end{aligned} \tag{65}$$

where the boundary term vanishes under standard boundary conditions (e.g. $h_{\mu\nu} \to 0$ at spatial infinity). Given the equivalence to the Einstein model, we adopt this well-known result directly.

From 2.3.4, deformation field action is in Equation (13):

Define the deformation field's energy-momentum tensor:

$$T_{\mu\nu} = -\frac{2}{\sqrt{-h}}\frac{\delta\left(\sqrt{-h}\mathcal{L}_{slice}\right)}{\delta h^{\mu\nu}} \tag{66}$$

So:

$$\begin{aligned}\delta S_{slice} &= \delta S_{grav} + \delta S_{deform} \\ &= \int \frac{c^4}{16\pi G}\left(R_{\mu\nu} - \frac{1}{2}h_{\mu\nu}R\right)\delta h^{\mu\nu}\sqrt{-h}\,\mathrm{d}^4x + \int \frac{\delta\left(\sqrt{-h}\mathcal{L}_{slice}\right)}{\delta h^{\mu\nu}}\delta h^{\mu\nu}\,\mathrm{d}^4x \\ &= \int \left[\frac{c^4}{16\pi G}\left(R_{\mu\nu} - \frac{1}{2}h_{\mu\nu}R\right) - \frac{1}{2}T_{\mu\nu}\right]\delta h^{\mu\nu}\sqrt{-h}\,\mathrm{d}^4x = 0\end{aligned} \tag{67}$$

Since $\delta h^{\mu\nu}$ is arbitrary, must:

$$\frac{c^4}{16\pi G}\left(R_{\mu\nu} - \frac{1}{2}h_{\mu\nu}R\right) - \frac{1}{2}T_{\mu\nu} = 0 \tag{68}$$

$$R_{\mu\nu} - \frac{1}{2}h_{\mu\nu}R = \frac{8\pi G}{c^4}T_{\mu\nu} \tag{69}$$

Therefore, EFE has been derived.

3.3.2. Incorporation of Dark Energy into the Effective Gravitational Field Equations

In Section 3.1.3, we established that dark energy in our deformation wave model arises as an intrinsic property of the 5D brane, driven by the membrane's wave speed $C_{brane} = \sqrt{\frac{T}{\rho}}$, where T is the brane's bulk modulus (units: J·m^{-4}) and ρ is the brane bulk density (units: $\text{J·m}^{-6}\text{·s}^{-2}$). This wave speed governs the long-term accelerated expansion of the 4D slice spacetimes during the membrane oscillation-dominated stage, analogous to the dark energy-dominated era in standard cosmology. We derived the dark energy density in Equation (39) and the corresponding cosmological constant-like term in Equation (38). This formulation provides a geometric origin for dark energy, eliminating the need for ad hoc scalar fields or vacuum energy assumptions, as required in the standard ΛCDM model. In this section, we incorporate this dark energy term into the effective gravitational field equations derived in Section 3.3.1, ensuring consistency with both the model's geometric foundation and cosmological observations, such as the dark energy fraction $\Omega_\Lambda \approx 0.7$.

Incorporation via the Gravitational Action:

To include dark energy in the effective field equations, we modify the gravitational action S_{grav} in the 4D slice to account for the cosmological constant-like term Λ. In standard General Relativity (GR), dark energy is introduced by adding a cosmological constant term to the Einstein-Hilbert action. Following this approach, we modify the gravitational action from Section 2.3.4 in Equation (12) to include the dark energy contribution:

$$S_{grav} = \int \mathrm{d}^4 x \sqrt{-h} \frac{1}{2\kappa_4} \left(R - 2\Lambda \right) \tag{70}$$

Here, the factor -2Λ is chosen to ensure that the resulting field equations align with the standard form in GR, where Λ appears as a cosmological constant. The total action for the 4D slice S_{slice} remains in Equation (11) with S_{deform} as defined in Section 2.3.4. in Equation (13). We follow the same derivation process as in 3.3.1 to obtain.

$$R_{\mu\nu} - \frac{1}{2} h_{\mu\nu} R + \Lambda h_{\mu\nu} = R_{\mu\nu} - \frac{1}{2} h_{\mu\nu} R + \frac{3T}{c^2 R_{n0}^2 \rho} h_{\mu\nu} = \frac{8\pi G}{c^4} T_{\mu\nu} \tag{71}$$

We definite:

$$G_{\mu\nu} = R_{\mu\nu} - \frac{1}{2} h_{\mu\nu} R \tag{72}$$

Then:

$$G_{\mu\nu} + \Lambda h_{\mu\nu} = G_{\mu\nu} + \frac{3T}{c^2 R_{n0}^2 \rho} h_{\mu\nu} = \frac{8\pi G}{c^4} T_{\mu\nu} \tag{73}$$

This is the modified Einstein Field Equation (EFE) in the 4D slice, now incorporating the dark energy term $\Lambda h_{\mu\nu}$, which matches the standard form in GR with a cosmological constant.

Physical Implications and Consistency with Observations:

The inclusion of the dark energy term $\Lambda h_{\mu\nu}$ in the EFE ensures that the 4D slice spacetimes exhibit accelerated expansion during the membrane oscillation-dominated stage, as described in Section 3.1.3. The Hubble parameter in this phase, given in Equation (36), matches the standard $H^2 = \Lambda c^2 / 3$, as shown in Section 3.1.3, confirming that our model reproduces the observed late-time acceleration. Using the observed dark energy density $\rho_{DE} \approx 7 \times 10^{-27}$ kg/m³, we can constrain the model parameters T, ρ and R_{n0}:

$$\rho_{DE} = \frac{3T}{8\pi G R_{n0}^2 \rho} = 7 \times 10^{-27}\ \mathrm{kg/m^3} \tag{74}$$

Given $G \approx 6.674 \times 10^{-11}\ \mathrm{m^3 \cdot kg^{-1} \cdot s^{-2}}$, this implies a relationship between the brane's bulk modulus, bulk density, and the scale R_{n0}, which can be further refined with observational data in future work. The dark energy fraction $\Omega_\Lambda \approx 0.7$ is naturally achieved by this density, aligning with cosmological observations.

In our model, dark energy is not an ad hoc addition but a direct consequence of the brane's intrinsic dynamics. The wave speed C_{brane} acts as a fundamental parameter, tying the accelerated expansion to the elastic properties of the 5D brane, offering a geometric explanation for dark energy that contrasts with the vacuum energy or scalar field approaches in standard cosmology.

Impact on the Deformation Wave Dynamics:

The dark energy term $\Lambda h_{\mu\nu}$ introduces a uniform negative pressure across the 4D slice, influencing the propagation of the deformation wave Φ. Specifically, this negative pressure arises from the intrinsic wave speed C_{brane}, which drives the expansion of the spatial extent of wave crests and troughs as the deformation wave propagates, mirroring the cosmic expansion observed in our universe. During the membrane oscillation-dominated stage, this term enhances the expansion of the wave crests and troughs, ensuring that matter-dominated universes (crests) and antimatter-dominated universes (troughs) continue to separate and evolve independently.

Comparison with Standard Cosmology:

In the standard ΛCDM model, dark energy is introduced as a cosmological constant Λ, with its origin often attributed to quantum vacuum fluctuations—a hypothesis that faces challenges such as the cosmological constant problem (the discrepancy between theoretical and observed values of Λ). In contrast, our model derives Λ from the brane's intrinsic properties, providing a physical mechanism for dark energy that avoids fine-tuning issues. The resulting field equations are mathematically equivalent to those in GR with a cosmological constant, ensuring consistency with observational tests of GR, such as the accelerated expansion inferred from Type Ia supernovae and the CMB power spectrum.

Future Directions:

While the current derivation successfully incorporates dark energy into the EFE, further work is needed to:

- Constrain the parameters T, ρ and R_{n0} using precise cosmological data, such as the Planck 2018 measurements of ρ_{DE} and Ω_Λ;
- Investigate the interaction between the dark energy term and the deformation field Φ, particularly how $\Lambda h_{\mu\nu}$ influences the formation of new wave crests and troughs in the multiverse framework;
- Explore potential time-variations in Λ, as the wave speed Cbrane may evolve with the brane's density ρ over cosmic timescales, offering a dynamic dark energy model.

In summary, the incorporation of dark energy into the effective gravitational field equations provides a unified geometric explanation for late-time cosmic acceleration, aligning with observational data while grounding dark energy in the intrinsic dynamics of the 5D brane.

3.3.3. The Geometric Origin of Dark Matter

In this section, we propose a novel mechanism for the origin of dark matter, rooted in the geometric dynamics of the 5D brane. The aggregation of microscopic deformation "knots" within the 4D slice spacetimes at wave crests and troughs induces macroscopic spacetime curvature. This curvature propagates non-locally through the connectivity of the 5D brane, affecting surrounding regions, including the inter-wave dark sectors. Through a positive feedback mechanism, this process leads to the accumulation of large-scale spacetime curvature, whose gravitational effects we identify as those of dark matter. We demonstrate how this geometric framework naturally produces dark matter, consistent with observational constraints such as the dark matter-to-baryon density ratio ($\frac{\rho_{DM}}{\rho_b} \approx 5$).

1) Aggregation of microscopic deformation knots and local spacetime curvature

Within the 4D slice spacetimes at wave crests and troughs (corresponding to matter- or antimatter-dominated universes, as discussed in Section 3.2), the microscopic deformation "knots" represent localized quantum excitations of gauge fields (e.g., photons, gluons; see Section 2.4). The aggregation of these knots within a 4D slice contributes directly to the Einstein Field Equations (EFE) through their energy-momentum tensor $T_{\mu\nu}^{knots}$, inducing local spacetime curvature:

$$G_{\mu\nu} = \frac{8\pi G}{c^4} T_{\mu\nu}^{knots} \tag{75}$$

where $T_{\mu\nu}^{knots}$ is the energy-momentum tensor of the knots.

When a large number of knots aggregate, their total energy-momentum tensor is $T_{\mu\nu}^{total} = \int T_{\mu\nu}^{knot}$, producing a local contribution to the Einstein tensor in the m-th slice:

$$G_{\mu\nu}^{local,(m)} = \frac{8\pi G}{c^4} \sum T_{\mu\nu}^{knots,(m)} \tag{76}$$

In the non-relativistic approximation, the dominant component of $T_{\mu\nu}^{knots,(m)}$ is the energy density, $\sum T_{00}^{knots,(m)} \approx \rho_{knots,(m)} c^2$, where $\rho_{knots,(m)}$ is the observable mass-energy density of the aggregated knots in the m-th slice. Thus, the corresponding component of the Einstein tensor is:

$$G_{00}^{local,(m)} = \frac{8\pi G}{c^2} \rho_{knots,(m)} \tag{77}$$

This local curvature, quantified by $G_{\mu\nu}^{local,(m)}$ is typically significant on small scales (e.g., stellar scales), but within a single 4D slice, its effects are localized and cannot directly account for the large-scale gravitational effects attributed to dark matter.

2) Non-local propagation of spacetime curvature and positive feedback

Due to the connectivity of the 5D brane (Section 2.1), the macroscopic curvature in the 4D slice spacetimes at wave crests or troughs, quantified by $G_{\mu\nu}^{local,(m)}$, is not an isolated phenomenon, as microscopic deformation knots. Instead, it affects adjacent regions to cause the corresponding macroscopic curvature, propagates non-locally through the brane's geometry, including the inter-wave dark sectors. Consequently, the curvature from the crest and troughs slice, initially described by $G_{\mu\nu}^{local,(m)}$, propagates through the brane to the dark sectors, inducing metric changes and resulting in spacetime curvature within these regions, $G_{\mu\nu}^{dark,(m)}$. The curvature in the dark sectors exerts a gravitational influence on deformation knots that have not reached extremal values (*i.e.*, where $\partial\Phi/\partial x^4 \neq 0$, as discussed in Section 3.2). This gravitational potential well attracts additional knots in the dark sectors to aggregate further, increasing the local energy-momentum tensor $T_{\mu\nu}^{DM,(m)}$ and thereby enhancing the curvature in the dark sectors and thus the Einstein tensor:

$$G_{\mu\nu}^{DM,(m)} = \frac{8\pi G}{c^4} T_{\mu\nu}^{DM,(m)} \tag{78}$$

This process establishes a positive feedback loop:

- Curvature attracts knots to aggregate.
- Aggregation increases $T_{\mu\nu}^{knots}$, further enhancing curvature.

This positive feedback extends the curvature deeper into the dark sectors and, through the brane's geometry, propagates to subsequent wave crest and trough 4D slice spacetimes, altering their metric and inducing additional spacetime curvature. So the total Einstein tensor in the subsequent slice, (m + 1)-th slice, $G_{\mu\nu}^{total,(m+1)}$ is:

$$G_{\mu\nu}^{total,(m+1)} = G_{\mu\nu}^{local,(m+1)} + G_{\mu\nu}^{DM,(m)} \tag{79}$$

3) Accumulation of curvature effects

The total Einstein tensor in the m-th slice, quantified by $G_{\mu\nu}^{total,(m)}$, propagates through the brane to subsequent crest and trough slices, leading to a cumulative effect. During propagation, the curvature experiences a net modification due to both the positive feedback in the dark sectors and the geometric decay during propagation across the brane. We denote the net modification factor as β_m (where β_m combines the amplification from positive feedback $f_{feedback}$ and the decay from propagation $f_{decayand}$, so $\beta_m \equiv f_{feedback}/f_{decay\ and}$ can be greater or less than 1 depending on the relative strengths of these effects). So the curvature $G_{\mu\nu}^{DM,(m)}$ from the dark sector following the m slice is:

$$G_{\mu\nu}^{DM,(m)} = \beta_m G_{\mu\nu}^{total,(m)} \tag{80}$$

$$\begin{aligned} G_{\mu\nu}^{total,(m+1)} &= G_{\mu\nu}^{local,(m+1)} + G_{\mu\nu}^{DM,(m)} = G^{local,(m+1)} + \beta_m G^{total,(m)} \\ &= G^{local,(m+1)} + \beta_m G^{local,(m)} + \beta_m \beta_{m-1} G^{total,(m-1)} \\ &= G^{local,(m+1)} + \sum_{j=1}^{m} \left(\prod_{i=j}^{m} \beta_i \right) G^{local,(j)} \end{aligned} \tag{81}$$

$$G_{\mu\nu}^{DM,(m)} = \sum_{j=1}^{m} \left(\prod_{i=j}^{m} \beta_i \right) G^{local,(j)} \tag{82}$$

The accumulated spacetime curvature produces additional gravitational effects via the EFE, equivalent to an additional energy-momentum tensor $T_{\mu\nu}^{DM}$, This accumulation process is analogous to the non-linear growth of large-scale structures in cosmology (e.g., the Zeldovich approximation), but here it is realized through the geometric propagation across the 5D brane.

From Equation (77), we obtain:

$$\begin{aligned} G_{00}^{total,(m+1)} &= G_{00}^{local,(m+1)} + \sum_{j=1}^{m}\left(\prod_{i=j}^{m}\beta_i\right)G_{00}^{local,(j)} \\ &= \frac{8\pi G}{c^2}\rho_{knots,(m+1)} + \frac{8\pi G}{c^2}\sum_{j=1}^{m}\left(\prod_{i=j}^{m}\beta_i\right)\rho_{knots,(j)} \end{aligned} \tag{83}$$

We definite $\rho_{total,(m+1)}$ as total apparent mass-energy density that:

$$G_{00}^{total,(m+1)} = \frac{8\pi G}{c^2}\rho_{total,(m+1)} \tag{84}$$

So:

$$G_{00}^{total,(m+1)} = \frac{8\pi G}{c^2}\rho_{total,(m+1)} = \frac{8\pi G}{c^2}\rho_{knots,(m+1)} + \frac{8\pi G}{c^2}\sum_{j=1}^{m}\left(\prod_{i=j}^{m}\beta_i\right)\rho_{knots,(j)} \tag{85}$$

We obtain:

$$\rho_{total,(m+1)} = \rho_{knots,(m+1)} + \sum_{j=1}^{m}\left(\prod_{i=j}^{m}\beta_i\right)\rho_{knots,(j)} \tag{86}$$

In our model, the baryon density $\rho_b \approx \rho_{knots,(m)}$, so:

$$G_{00}^{DM,(m)} = \sum_{j=1}^{m}\left(\prod_{i=j}^{m}\beta_i\right)G_{00}^{local,(j)} = \frac{8\pi G}{c^2}\sum_{j=1}^{m}\left(\prod_{i=j}^{m}\beta_i\right)\rho_{b,(j)} \tag{87}$$

$$\rho_{total,(m+1)} \approx \rho_{b,(m+1)} + \sum_{j=1}^{m}\left(\prod_{i=j}^{m}\beta_i\right)\rho_{b,(j)} \tag{88}$$

For dark matter density $\rho_{DM,(m+1)}$, we have:

$$\rho_{total,(m+1)} \approx \rho_{b,(m+1)} + \rho_{DM,(m+1)} = \rho_{b,(m+1)} + \sum_{j=1}^{m}\left(\prod_{i=j}^{m}\beta_i\right)\rho_{b,(j)} \tag{89}$$

$$\rho_{DM,(m+1)} = \sum_{j=1}^{m}\left(\prod_{i=j}^{m}\beta_i\right)\rho_{b,(j)} \tag{90}$$

$$\frac{\rho_{DM,(m+1)}}{\rho_{b,(m+1)}} = \frac{\sum_{j=1}^{m}\left(\prod_{i=j}^{m}\beta_i\right)\rho_{b,(j)}}{\rho_{b,(m+1)}} \tag{91}$$

With appropriate values of m (the number of predecessor universes), β_i (the net modification factor of i-th universe) and $\rho_{b,(j)}$ (the baryon density in j-th universe), this ratio can naturally align with the observed value of $\frac{\rho_{DM}}{\rho_b} \approx 5$ without requiring precise tuning, thus maintaining a natural and physically motivated framework. More detailed quantitative studies will be carried out in subsequent work.

In our model, dark matter arises not from unknown particles within our current universe, but as a cumulative geometric memory of preceding universes—wave crests and troughs that formed earlier along the deformation wave. Each former universe, indexed by $j = 1, 2, \cdots, m$, contributes residual curvature traces $\rho_b^{(j)}$, corresponding to its baryonic matter density. These residual effects are geometrically projected onto the current wave crest (our universe), but each is modified by a factor β_i, which accounts for curvature dispersion and the damping effect of inter-wave energy storms. The dark matter density equation defined previously in our universe encodes the hierarchical inheritance of geometric deformation traces, A higher number of prior universes (larger m) naturally leads to more accumulated dark matter, while geometric screening suppresses short-wavelength curvature features, resulting in a smooth, non-clustering dark component consistent with observations. The existence of the gravitational effect of dark matter indicates that there were several predecessor universes before our universe.

4) Scale-dependent effects of energy storms

In the inter-wave dark sectors, tachyonic instabilities of the gauge fields (Section 3.2.3) lead to a negative effective mass, $\mathcal{M}_{eff}^2(\Phi) = -\lambda\left(\frac{\partial V_{brane}}{\partial x^4}\right)^2$, causing exponential growth of perturbations in Equations (60) and (61).

This rapid growth of tachyonic modes triggers violent local energy fluctuations, termed "energy storms." These energy storms result in:

- Rapid changes in the gauge field energy density;
- Violent energy fluctuations in localized regions;
- A persistent state of energy storms, disrupting the stability of small-scale spacetime structures.

Specifically, energy storms disrupt the spacetime curvature induced by knot aggregation on small scales (e.g., stellar scales). For instance, on stellar scales, the gravitational potential from knot aggregation is $\Phi_{grav} \sim -\frac{GM}{r}$, but the violent fluctuations from energy storms prevent these small-scale structures from remaining stable, effectively smoothing out the spacetime curvature.

However, on large scales (e.g., galactic scales), the impact of energy storms is limited. The growth timescale of energy storms, $\tau \sim 1/\gamma$, is short (Section 3.2.3), confining their effects to localized regions. Consequently, large-scale curvature can accumulate before being disrupted by energy storms, resulting in persistent gravitational effects. This scale-dependent behavior aligns with cosmological observations of structure formation: dark matter effects are negligible on small scales (e.g., stellar scales), but dominate on large scales (e.g., galactic scales), as evidenced by galaxy rotation curves.

5) Further consistency with observations

The gravitational effects of accumulated curvature in the dark sectors, quantified by $G_{\mu\nu}^{DM}$, influence the geometry of the 4D slice, enhancing large-scale curvature in a manner consistent with CMB density fluctuations ($n_s \approx 0.96$, Section 3.1). Additionally, this mechanism is compatible with the holographic principle: geometric changes on the 5D brane project onto the 4D slice, producing additional gravitational effects, akin to non-local gravitational propagation in the AdS/CFT [26] correspondence.

Compared to the standard cold dark matter (CDM) model in cosmology, our framework treats dark matter as a geometric effect rather than a particle species.

This geometric origin circumvents challenges in the CDM model, such as the lack of significant signals in direct detection experiments for dark matter particles (e.g., WIMPs). Furthermore, the dynamics of the brane provide a testable framework: the distribution of accumulated curvature may leave observable imprints in CMB anisotropies or large-scale structure, which can be probed by next-generation telescopes such as Euclid and LSST.

6) Comparison with ΛCDM and DGP Models

Compared to the ΛCDM model, which treats dark matter as a cold, non-relativistic particle species and dark energy as a vacuum energy component, our geometric framework provides a unified origin from spacetime deformation [27]. The scalar spectral index $n_s \approx 0.96$, dark matter-to-baryon ratio $\frac{\rho_{DM}}{\rho_b} \approx 5$, and dark energy density $\Omega_\Lambda \approx 0.7$ emerge naturally from geometric quantities such as the brane wave speed C_{brane}, bulk modulus *T*, and bulk density ρ.

Unlike the Dvali-Gabadadze-Porrati (DGP) model, which modifies gravity via a 4D brane embedded in a 5D Minkowski bulk with a crossover scale r_c, our model retains General Relativity on the 4D slice and derives its Einstein equations from brane elasticity. There is no need for ghost-free constraints or infrared modifications of gravity.

This model circumvents key limitations of ΛCDM and DGP by providing physically motivated origins for all cosmic components—gravity, dark matter, and dark energy—within a single geometric brane structure.

7) Future directions

While the current model qualitatively aligns with the observational characteristics of dark matter, further quantitative analysis is required:

- Precise Calculation of Dark Matter Density: Numerical simulations should be conducted to compute $G_{\mu\nu}^{DM}$ across the dark sectors, verifying the resulting ρ_{DM} against the observed value of $\rho_{DM} \approx 1.3\times10^{-27}$ kg/m³ (corresponding to $\Omega_{DM} \approx 0.27$, Planck 2018 data [7]).
- Dynamics of Non-Local Propagation: A detailed study of the net modification factor β during propagation across the brane is needed to quantify its impact on curvature accumulation.
- Energy Storms: Further investigation into the growth timescale $\tau \sim 1/\gamma$ of energy storms is warranted to understand their effects on curvature accumulation at different scales.
- Observational Tests: The gravitational effects of accumulated curvature should be examined for their impact on galaxy rotation curves, gravitational lensing, and the CMB power spectrum, with comparisons to predictions from the standard CDM model.

8) Summary

This section proposes a geometric origin for dark matter's gravitational effects through the aggregation of microscopic deformation knots in 4D slice spacetimes at wave crests and troughs, the non-local propagation of spacetime curvature, the scale-dependent effects of energy storms. The spacetime curvature, quantified by the Einstein tensor $G_{\mu\nu}^{DM}$, accumulates through propagation and feedback in the dark sectors, producing gravitational effects equivalent to dark matter. The resulting density ratio, ρ_{DM}/ρ_b, can naturally align with observations ($\frac{\rho_{DM}}{\rho_b} \approx 5$) for appropriate values of the number of predecessor universes, the net modification factor and the baryon density in predecessor universe. This mechanism not only provides a unified geometric framework for explaining the origin of dark matter but also aligns with CMB observations and the holographic principle, offering testable predictions for future observations.

4. Conclusions

In this work, we have introduced a novel deformation wave model of brane cosmology, where a 5D membrane embedded in a 6D bulk spacetime undergoes intrinsic geometric deformations triggered by a Gaussian perturbation. This model provides a unified geometric framework that derives the Einstein Field Equations (EFE), explains the origins of dark matter and dark energy, and accounts for the formation of a finite multiverse, all without invoking ad hoc scalar fields or fine-tuned parameters prevalent in traditional brane-world scenarios. Our approach addresses fundamental questions in cosmology, offering a physically motivated mechanism for spacetime curvature, unifying gravity, matter, dark matter, and dark energy within a single geometric construct.

The three-stage cosmic evolution delineated in Section 3.1—inflation zone, transition, and membrane oscillation-dominated stages—demonstrates how the deformation wave drives the formation of a "universe factory." Stable 4D slice spacetimes emerge at wave crests (matter-dominated universes) and troughs (antimatter-dominated universes), with their isotropy and near-scale-invariant density fluctuations ($n_s \approx 0.96$) aligning with Cosmic Microwave Background (CMB) observations. The inflation zone, driven by high-energy Gaussian perturbations, achieves an expansion factor consistent with standard cosmology ($\sim 10^{26}$) without requiring a reheating phase, presenting a "hot inflation" scenario. The transition stage converts shock wave energy into intrinsic brane oscillations, while the membrane oscillation-dominated stage reproduces late-time cosmic acceleration through the brane's wave speed $C_{brane} = \sqrt{\frac{T}{\rho}}$, yielding a dark energy density ($\rho_{DE} = \frac{3T}{8\pi G R_{n0}^2 \rho}$) that matches the observed value ($\Omega_\Lambda \approx 0.7$).

A key innovation of our model lies in the geometric derivation of the EFE (Section 3.3.1), where gravity emerges as a macroscopic response to the cumulative pressure of microscopic deformation "knots" propagating along the brane. This derivation roots spacetime curvature in the brane's elastic dynamics, addressing a fundamental gap in GR by providing a physical mechanism for the EFE. Dark energy is incorporated as a cosmological constant-like term ($\Lambda = \frac{3C_{brane}^2}{c^2 R_{n0}^2}$)

derived from the brane's intrinsic properties, eliminating the need for vacuum energy assumptions and mitigating fine-tuning issues associated with the cosmological constant problem.

Dark matter, as proposed in Section 3.3.3, arises from the non-local propagation and accumulation of spacetime curvature through the 5D brane's connectivity. The curvature, initially induced by the aggregation of deformation knots in wave crest and trough slices, propagates to inter-wave dark sectors, where a positive feedback mechanism enhances its effects. The accumulated curvature, quantified by the Einstein tensor $G_{\mu\nu}^{DM}$, produces gravitational effects equivalent to dark matter, with a density ratio $\frac{\rho_{DM}}{\rho_b} \approx 5$ that can naturally align with observations given appropriate values of the number of predecessor universes, the net modification factor and the baryon density in predecessor universes. This geometric origin of dark matter circumvents challenges faced by the standard cold dark matter (CDM) model, such as the absence of direct detection signals for dark matter particles (e.g., WIMPs), and aligns with cosmological observations like galaxy rotation curves and large-scale structure formation, where dark matter effects dominate on galactic scales but are negligible on stellar scales due to the disruptive effects of energy storms.

The model's consistency with key cosmological observations [28]—including the CMB scalar spectral index ($n_s \approx 0.96$), the dark matter-to-baryon density ratio ($\frac{\rho_{DM}}{\rho_b} \approx 5$), and the dark energy fraction ($\Omega_\Lambda \approx 0.7$)—underscores its viability as an alternative to the ΛCDM paradigm. Furthermore, the framework is compatible with the holographic principle, as geometric changes on the 5D brane project onto the 4D slice, producing non-local gravitational effects akin to those in the AdS/CFT [26] correspondence. The cyclic nature of the "universe factory" also predicts a finite multiverse, with potential signatures in CMB anisotropies that can be probed by next-generation telescopes such as Euclid and LSST.

Despite these promising results, we acknowledge that the current work remains a preliminary theoretical framework, with certain aspects requiring further refinement due to time and computational constraints. Specifically, the quantum characteristics of the deformation "knots" (e.g., their wave function forms and interactions) are only qualitatively described, lacking a detailed quantum field theory framework. Additionally, the quantitative analysis of dark matter density (ρ_{DM}) and the specific forms of observable predictions (e.g., corrections to the CMB power spectrum) are not fully developed, as they require extensive numerical simulations and observational data analysis. These limitations do not undermine the core conceptual framework of the model but highlight the need for further investigation to enhance its predictive power and robustness.

To address these shortcomings, we outline a comprehensive plan for future research. First, we will develop a quantum field theory framework for the deformation "knots," deriving their wave functions and interaction Lagrangian to rigorously quantify their role as the source of matter and dark matter. This quantumization study aims to bridge quantum mechanics and relativity theory, providing a unified description of the deformation "knots" that integrates the microscopic quantum behavior with the macroscopic gravitational effects observed in the 4D slice spacetimes. This will involve constructing a scalar field quantization model for Φ and calculating its energy density contributions. Second, we plan to conduct numerical simulations to compute the accumulated Einstein tensor $G_{\mu\nu}^{DM}$ across the dark sectors, using high-performance computing resources to determine the dark matter density ρ_{DM} and verify its consistency with the observed value ($\rho_{DM} \approx 1.3\times10^{-27}$ kg/m^3). These simulations will also allow us to constrain the model parameters (T, ρ , R_{n0}) by comparing the derived dark energy density ρ_{DE} with Planck 2018 measurements ($\rho_{DE} \approx 7\times10^{-27}$ kg/m^3). Third, we will calculate specific observable signatures, such as the corrections to the CMB power spectrum induced by the multiverse structure, and compare these predictions with data from upcoming experiments like Euclid and LSST. Additionally, we aim to quantify the growth timescale of energy storms ($\tau \sim 1/\gamma$) and their scale-dependent effects on spacetime curvature, further refining the model's explanation of dark matter's behavior at different scales. These future studies will build upon the foundation established in this work, providing a more complete and testable framework for brane cosmology.

The physical picture of our deformation wave model reveals a unique interplay of determinism and non-determinism in the distribution of cosmic matter across different scales. On large scales (e.g., galactic scales), due to the propagation characteristics of the deformation wave, the predecessor and successor universes act as parallel universes positioned at different temporal locations, exhibiting a deterministic evolution governed by the wave's cyclic nature. In contrast, on small scales (e.g., stellar scales), the disruptive effects of energy storms on spacetime curvature traces cause the predecessor and successor universes to evolve independently, introducing a non-deterministic component to their dynamics. This combination of deterministic and non-deterministic behaviors offers a novel perspective on the cosmic matter distribution, potentially providing new insights into the structure and evolution of the universe.

In conclusion, the deformation wave model of brane cosmology offers a compelling alternative to traditional frameworks by unifying gravity, dark matter, and dark energy within a single geometric paradigm. Compared to models that introduce dark components as separate entities, our geometric construction integrates all cosmic ingredients as dynamic manifestations of brane deformation. Importantly, while Equation (10) differs in form from the traditional Einstein field equations (EFE), it encapsulates the same fundamental principle that spacetime curvature is determined by the local distribution of matter and energy. This relationship provides a physically motivated explanation for how deformation knots generate curvature, offering insights beyond purely geometric postulates such as the Einstein-Hilbert action.

An essential and distinctive feature of our framework is the multi-layered structure of the universe, where successive 4D slices corresponding to wave crests and troughs are nested concentrically like a series of Russian dolls, all originating from a common inflationary core. Unlike parallel universes envisioned in many multiverse scenarios, these layers are embedded within one another, forming a nested cosmic architecture in which each layer constitutes a complete universe while simultaneously participating in a larger interconnected higher-dimensional structure.

Although the current study represents a preliminary step that requires further development in mathematical rigor, quantitative analysis, and observational predictions, its conceptual innovation and preliminary consistency with known cosmological phenomena demonstrate significant potential for advancing our understanding of the universe. Future research will address the identified limitations, aiming to develop this model into a robust and predictive framework capable of withstanding rigorous observational tests.

Conflicts of Interest

The authors declare no conflicts of interest regarding the publication of this paper.

References

[1] Randall, L. and Sundrum, R. (1999) Large Mass Hierarchy from a Small Extra Dimension. *Physical Review Letters*, **83**, 3370-3373. https://doi.org/10.1103/physrevlett.83.3370

[2] Randall, L. and Sundrum, R. (1999) An Alternative to Compactification. *Physical Review Letters*, **83**, 4690-4693. https://doi.org/10.1103/physrevlett.83.4690

[3] Hořava, P. and Witten, E. (1996) Heterotic and Type I String Dynamics from Eleven Dimensions. *Nuclear Physics B*, **460**, 506-524. https://doi.org/10.1016/0550-3213(95)00621-4

[4] Antoniadis, I., Arkani-Hamed, N., Dimopoulos, S. and Dvali, G. (1998) New Dimensions at a Millimeter to a Fermi and Superstrings at a TEV. *Physics Letters B*, **436**, 257-263. https://doi.org/10.1016/s0370-2693(98)00860-0

[5] Polchinski, J. (1998) String Theory. Cambridge University Press. https://doi.org/10.1017/cbo9780511816079

[6] Guth, A.H. (1981) Inflationary Universe: A Possible Solution to the Horizon and Flatness Problems. *Physical Review D*, **23**, 347-356. https://doi.org/10.1103/physrevd.23.347

[7] Akrami, Y., Arroja, F., Ashdown, M., Aumont, J., Baccigalupi, C., Ballardini, M., *et al.* (2020) Planck 2018 Results: X. Constraints on Inflation. *Astronomy & Astrophysics*, **641**, A10. https://doi.org/10.1051/0004-6361/201833887

[8] Dick, R. (2001) Standard Cosmology and the Bulk Universe. arXiv: hep-th/0110162.

[9] Kim, H.B. (2001) Brane-World Phenomenology: From Cosmology to Particle Physics. arXiv: hep-ph/0102182.

[10] Dodelson, S. and Schmidt, F. (2020) Modern Cosmology. 2nd Edition, Academic Press. https://doi.org/10.1016/C2017-0-01943-2

[11] Weinberg, S. (2008) Cosmology. Oxford University Press. https://doi.org/10.1093/oso/9780198526827.001.0001

[12] DeWolfe, O., Freedman, D.Z., Gubser, S.S. and Karch, A. (2000) Modeling the Fifth Dimension with Scalars and Gravity. *Physical Review D*, **62**, Article ID: 046008. https://doi.org/10.1103/physrevd.62.046008

[13] Dvali, G., Gabadadze, G. and Porrati, M. (2000) 4D Gravity on a Brane in 5D Minkowski Space. *Physics Letters B*, **485**, 208-214. https://doi.org/10.1016/s0370-2693(00)00669-9

[14] Maartens, R. (2004) Brane-World Gravity. *Living Reviews in Relativity*, **7**, Article No. 7. https://doi.org/10.12942/lrr-2004-7

[15] Lehoucq, R., Weeks, J., Uzan, J., Gausmann, E. and Luminet, J. (2002) Eigenmodes of Three-Dimensional Spherical Spaces and Their Application to Cosmology. *Classical and Quantum Gravity*, **19**, 4683-4708. https://doi.org/10.1088/0264-9381/19/18/305

[16] Coleman, S. (1985) Q-balls. *Nuclear Physics B*, **262**, 263-283. https://doi.org/10.1016/0550-3213(85)90286-x

[17] Wesson, P.S. (1999) Space-Time-Matter: Modern Kaluza-Klein Theory. World Scientific. https://doi.org/10.1142/3889

[18] Overduin, J.M. and Wesson, P.S. (1997) Kaluza-Klein Gravity. *Physics Reports*, **283**, 303-378. https://doi.org/10.1016/s0370-1573(96)00046-4

[19] Langlois, D. (2002) Brane Cosmology. *Progress of Theoretical Physics Supplement*, **148**, 181-212. https://doi.org/10.1143/ptps.148.181

[20] Alencar, G., Landim, R.R., Tahim, M.O. and Costa Filho, R.N. (2014) Gauge Field Localization on the Brane through Geometrical Coupling. *Physics Letters B*, **739**, 125-127. https://doi.org/10.1016/j.physletb.2014.10.040

[21] Pease, R. (2001) Brane New World. *Nature*, **411**, 986-988. https://doi.org/10.1038/35082684

[22] Csáki, C., Grojean, C., Pilo, L. and Terning, J. (2004) Towards a Realistic Model of Higgsless Electroweak Symmetry Breaking. *Physical Review Letters*, **92**, Article ID: 101802. https://doi.org/10.1103/physrevlett.92.101802

[23] Liddle, A.R. and Lyth, D.H. (2000) Cosmological Inflation and Large-Scale Structure. Cambridge University Press. https://doi.org/10.1017/cbo9781139175180

[24] Bekenstein, J.D. (2004) Relativistic Gravitation Theory for the Modified Newtonian Dynamics Paradigm. *Physical Review D*, **70**, Article ID: 083509. https://doi.org/10.1103/physrevd.70.083509

[25] Sypsas, S. (2014) Theoretical and Observational Constraints on Brane Inflation and Study of Scalar Perturbations through the Effective Field Theory Formalism. arXiv: 1406.0939.

[26] Gubser, S.S. (2001) AdS/CFT and Gravity. *Physical Review D*, **63**, Article ID: 084017. https://doi.org/10.1103/physrevd.63.084017

[27] Clifton, T., Ferreira, P.G., Padilla, A. and Skordis, C. (2012) Modified Gravity and Cosmology. *Physics Reports*, **513**, 1-189. https://doi.org/10.1016/j.physrep.2012.01.001

[28] Ade, P.A.R., Aghanim, N., Arnaud, M., Ashdown, M., Atrio-Barandela, F., Aumont, J., *et al.* (2013) Planck Intermediate Results: IX. Detection of the Galactic Haze with Planck. *Astronomy & Astrophysics*, **554**, A139. https://doi.org/10.1051/0004-6361/201220271

Appendix A. Emergence of Macroscopic Spacetime Curvature from Deformation Knots

1) Physical Motivation

In the proposed model, "deformation knots" represent localized geometric distortions propagating along the fifth spatial dimension x^4, embedded within a five-dimensional brane world. Each knot corresponds to a microscopic excitation of the brane's internal structure, contributing a localized energy density and geometric perturbation. While individual knots induce only small spacetime distortions, their cumulative effect over large regions leads to measurable macroscopic spacetime curvature.

This appendix formalizes the idea that macroscopic Ricci scalar curvature $R(x)$ arises not from a single knot, but from the superposition of geometric influences of all knots across the brane, modulated by their geodesic separation or causal connectivity from the evaluation point.

2) Mathematical Expression of Curvature as an Integral

We assume that each deformation knot located at position x' contributes to the curvature at point x via a kernel function $K(x,x')$, which decays with increasing distance $|x-x'|$. The local Ricci scalar $R(x)$ is then expressed as:

$$R(x)=\int_{\mathcal{M}} K(x,x')\Phi(x')\mathrm{d}^4x' \tag{A1}$$

where:

- $\mathcal{M}$ is the 4D spacetime slice of the brane;
- $\Phi(x')$ is the scalar deformation amplitude associated with deformation knots at point x';
- $K(x,x')$ is a propagator kernel (e.g., Green's function), satisfying the condition:

$$\lim_{|x-x'|\to\infty} K(x,x')=0 \tag{A2}$$

This integral formulation reflects the nonlocal and cumulative nature of curvature generation in the presence of microstructural brane excitations.

3) Choice of Kernel Function

In different regimes, the kernel K may take various forms:

- In flat-space approximation: $K(x,x')\propto \dfrac{1}{|x-x'|^2}$.
- With exponential damping (screening): $K(x,x')\propto \dfrac{\mathrm{e}^{-\mu|x-x'|}}{|x-x'|}$.
- From linearized Einstein gravity: $K(x,x')=G_{\text{ret}}(x-x')$, the retarded Green's function.

The choice of kernel depends on the brane's geometric and dynamic properties.

4) Implications for Equation (10)

In this framework, we define $\varepsilon_\Phi(x)$ as the local energy density of the deformation field at point x on the brane. Physically, this energy arises from microscopic longitudinal deformation knots propagating within the connected 5D brane. Due to the intrinsic nonlocality of the brane-embedded in a higher-dimensional bulk-the energy at a single point is influenced not only by the local deformation field, but also by remote deformations throughout the brane.

To account for this, we define the deformation field energy density as a nonlocal functional of the deformation knot distribution:

$$\varepsilon_{\Phi}(x) = k\int_{\mathcal{M}} K(x, x')\Phi(x')\mathrm{d}^4 x' \tag{A3}$$

where k is a positive constant reflecting the proportional relation between deformation and local energy density.

Thus, by direct substitution of (A1), the deformation field energy density and the scalar curvature are proportional:

$$\varepsilon_{\Phi}(x) = kR(x) \tag{A4}$$

This naturally leads to the key result in Equation (10) of the main text.

$\varepsilon_{\Phi}(x)$ encapsulates the macroscopic energy response induced by microscopic geometric deformations, encoded through the emergent Ricci scalar curvature. This bridges the local physical energy interpretation with the emergent geometric framework of brane gravity. Unlike traditional point-sourced gravity, this model attributes geometric curvature to collective brane excitations, offering a potential geometric origin of gravity without invoking classical mass sources.

Appendix B. Python Simulation Code for Inflation Dynamics in Deformation Field Model

1. Code

Listing 1: Simulation Code

```python
import numpy as np
import matplotlib.pyplot as plt
from mpmath import mp, mpf, exp, sqrt

# Set high precision for calculations
mp.dps = 50

# --- Physical constants and parameters ---
C = mpf("2.05e47")          # Fixed inflation parameter C [m/s]
R0 = mpf("1e-12")           # Initial radius of the universe [m]
tau = mpf("1.78e-32")       # Characteristic inflation timescale [s]

# --- Time setup ---
num_points = 100000
t = np.linspace(0, 1e-32, num_points)

# --- Initialize storage for calculated values ---
R_vals, dotR_vals, ddotR_vals, epsilon_vals, ns_vals = [], [], [], [], []
R_current = R0

# --- Main calculation loop ---
for i in range(len(t)):
    t_mp = mpf(t[i])
    exp_term = exp(-t_mp**2 / (2 * tau**2))
    sqrt_term = sqrt(1 - exp_term)
    dotR = C * sqrt_term
    dotR_vals.append(float(dotR))
    if sqrt_term > 1e-20:
        ddotR = (t_mp * C * exp_term) / (tau**2 * sqrt_term)
    else:
        ddotR = mpf(0)
    ddotR_vals.append(float(ddotR))
    if i > 0:
        dt = t[i] - t[i - 1]
        R_current += 0.5 * (dotR + mpf(dotR_vals[i - 1])) * dt
    R_vals.append(float(R_current))
    if dotR != 0:
        epsilon = 1 - (ddotR * R_current) / (dotR ** 2)
    else:
        epsilon = mpf('inf')
    epsilon_vals.append(float(epsilon))
    ns = 1 - 2 * epsilon if epsilon != mpf('inf') else float('-inf')
    ns_vals.append(float(ns))

# --- Post-processing results ---
R_initial = R_vals[0]
R_final = R_vals[-1]
inflation_factor = R_final / R_initial
ns_valid = [val for val in ns_vals if 0 < val < 2]
```

```
average_ns = sum(ns_valid) / len(ns_valid)

# -- Plotting --
fig, axes = plt.subplots(5, 1, figsize=(12, 24), sharex=True)
axes[0].plot(t, dotR_vals)
axes[0].set_ylabel(r'$\dot{R}(t)$ [m/s]')
axes[0].set_title("1. Expansion Velocity $\dot{R}(t)$")
axes[1].plot(t, ddotR_vals)
axes[1].set_ylabel(r'$\ddot{R}(t)$ [m/s$^2$]')
axes[1].set_title("2. Acceleration $\ddot{R}(t)$")
axes[2].plot(t, R_vals)
axes[2].set_ylabel(r'$R(t)$ [m]')
axes[2].set_title("3. Scale Factor $R(t)$")
axes[3].plot(t, epsilon_vals)
axes[3].set_ylabel(r'$\epsilon(t)$')
axes[3].set_title("4. Slow-Roll Parameter $\epsilon(t)$")
axes[4].plot(t, ns_vals)
axes[4].set_ylim(0.8, 1)
axes[4].set_ylabel(r'$n_s(t)$')
axes[4].set_xlabel("Time t [s]")
axes[4].set_title("5. Scalar Spectral Index $n_s(t)$")
plt.tight_layout()
plt.show()

# -- Output key quantities --
{
 "The initial scale of cosmic inflation (m)": R_initial,
"The scale at the end of the cosmic inflationary explosion (m)" : f"{R_final:.18e}",
"The expansion factor of the inflationary ": inflation_factor,
"The average scalar spectral index of the inflationary": average_ns
}
```

The Python simulation code used to generate the figure is included in the supplementary file `simulation.py`.

2. Result

- The initial scale of cosmic inflation (in meters): $R_{\text{initial}} = 1.0 \times 10^{-12}$ m.
- The scale at the end of the cosmic inflationary explosion (in meters): $R_{\text{final}} = 3.99 \times 10^{14}$ m.
- The total expansion factor during inflation: $\frac{R_{\text{final}}}{R_{\text{initial}}} = 3.99 \times 10^{26}$.
- The average scalar spectral index of the inflationary phase: $n_s = 0.9607$.

The following is an evolutionary diagram of cosmic inflation parameters.

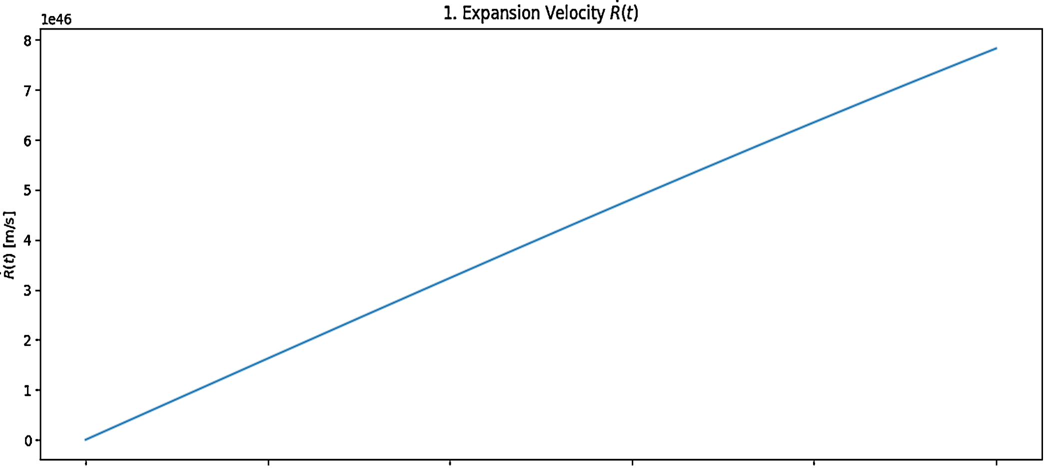

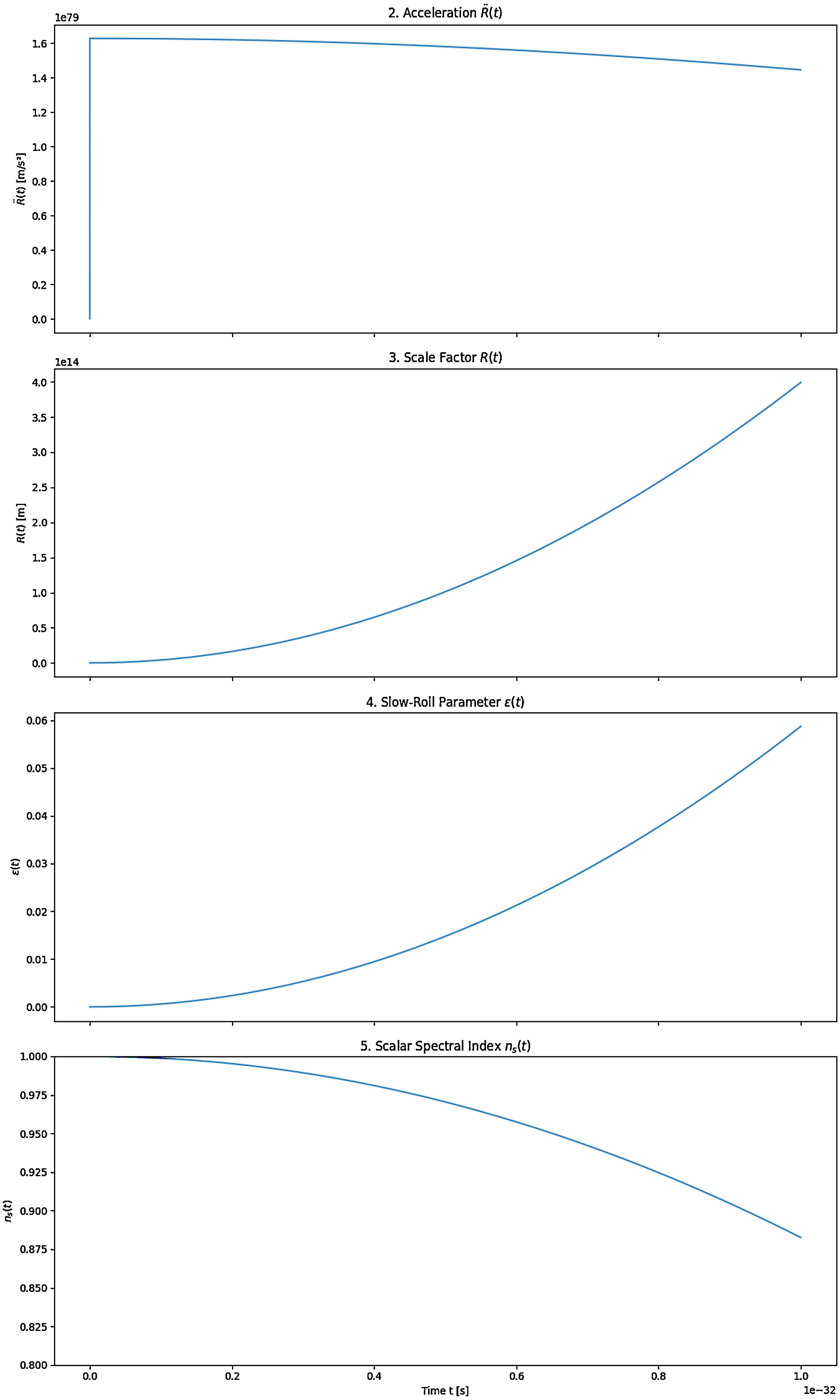
2. Acceleration $\ddot{R}(t)$
1e79
$\ddot{R}(t)$ [m/s²]
1.6
1.4
1.2
1.0
0.8
0.6
0.4
0.2
0.0
3. Scale Factor $R(t)$
1e14
$R(t)$ [m]
4.0
3.5
3.0
2.5
2.0
1.5
1.0
0.5
0.0
4. Slow-Roll Parameter $\varepsilon(t)$
$\varepsilon(t)$
0.06
0.05
0.04
0.03
0.02
0.01
0.00
5. Scalar Spectral Index $n_s(t)$
$n_s(t)$
1.000
0.975
0.950
0.925
0.900
0.875
0.850
0.825
0.800
0.0
0.2
0.4
0.6
0.8
1.0
1e−32
Time t [s]